Zirconium Alloy Getter Bed
Air-Ingress Thermal Failure Analysis

by

Valerie A. Hovland

Submitted to the Department of Mechanical Engineering in
Partial Fulfillment of the Requirements for the Degrees of

Master of Science in Mechanical Engineering
and
Bachelor of Science in Mechanical Engineering

at the
Massachusetts Institute of Technology
June 1998

Signature of Author_____
Department of Mechanical Engineering
December 19, 1997

Certified by_____
Charles Walthers
Engineer
Thesis Advisor, Los Alamos National Laboratory

Certified by_____
John H. Lienhard
Associate Professor of Mechanical Engineering
Thesis Advisor, MIT

Accepted by_____
Ain A. Sonin
Chairman, Department Committee on Graduate Studies, MIT

Zirconium Alloy Getter Bed
Air-Ingress Thermal Failure Analysis

by

Valerie A. Hovland

Submitted to the Department of Mechanical Engineering
on December 19, 1997 in partial fulfillment of the
requirements for the Degrees of Master of Science and
Bachelor of Science in Mechanical Engineering

ABSTRACT

In the event of an unexpected inrush of air into a packed St-909 getter bed, the exothermic reaction of oxygen and pellet material pushes temperatures within the bed to extremely high levels. This failure mode, which could be caused by a line rupture, was modeled, analyzed, and a full-scale experiment was performed in the Tritium Science and Engineering group at Los Alamos National Laboratory to confirm the results that the primary bed container will not fail from overheating. The oxidation of St-909 pellets was modeled and determined to be limited by the oxide diffusing into the pellet material. An effective diffusivity of the oxide into the pellet and its variance with temperature was determined. In the full-scale experiment, air was pumped through the bed at 15 standard liters per minute. Oxygen breaking through the bed was gradual and began after almost one hour of air flow. Maximum temperatures along the centerline of the bed reached 1280°C, primary container temperatures reached 840°C, and the primary container maintained structural integrity throughout the experiment.

Thesis Advisor, Charles Walthers, Los Alamos National Laboratory
Title: Engineer

Thesis Advisor, John H. Lienhard, MIT
Title: Associate Professor of Mechanical Engineering

Table of Contents

Chapter		*Page*
1	Introduction	5
	1.1 Overview	6
	1.2 Experimental Setup	6
2	Models of St-909 Bed	9
	2.1 Fundamental Equations Describing Solid and Fluid Temperatures	9
	2.2 One Dimensional Finite Difference Model	10
	2.2.1 Fluid Control Volume	11
	2.2.2 Solid Control Volume	13
	2.3 Axisymmetric Model	14
	2.4 Initial Conditions: Steady State Packed Bed Model	18
	2.4.1 Steady State Initial Temperatures	19
	2.5 Boundary Conditions	21
	2.5.1 Axial—Inlet Fluid Temperature	21
	2.5.2 Axial—Outlet Fluid Temperature	21
	2.5.3 Radial—Radiation	21
3	Oxide Diffusion Limiting (ODL) Model for Oxidation of St-909 Pellets	22
	3.1 ODL Theoretical Solution	22
	3.2 Small-Scale Experiments	23
	3.3 Determination of Pellet Radius Variation	25
	3.4 ODL Model Comparison to Experiments	26
4	Model Solution	27
	4.1 Equations for Solid and Fluid Temperatures	27
	4.1.1 One Dimensional Model	27
	4.1.2 Axisymmetric Model	27
	4.1.3 Temperature Solution	29
	4.2 C Program Steps for Solving Finite Difference Model	30
5	Results	31
	5.1 One Dimensional Predictions	31
	5.2 Axisymmetric Predictions	32
	5.3 Experimental Results	34
	5.4 Comparison between Theory and Experiment	36
6	Conclusions	40
	Nomenclature	41
	List of Works Cited	42

Appendices		
A	Summary of Experimental Results	43
B	Thermal Properties of Air versus Temperature	49
C	Heat Generation within Pellets	52
D	Stainless Steel Emissivity versus Temperature	55
E	Axisymmetric Model C Code	57

List of Figures and Tables

Title	*Page*
Figure 1: Glovebox Flow Loop	5
Figure 2: Getter Bed System	6
Figure 3: Schematic of Full-Scale Experiment	7
Figure 4: Full-Scale Experimental Setup	8
Figure 5: 1-D Differential Control Volume	9
Figure 6: Getter Bed in 50 Slices	10
Figure 7: 1D Finite Difference Model	11
Figure 8: Getter Bed in Axial and Radial Sections	14
Figure 9: Axisymmetric Finite Difference Model	15
Figure 10: Actual and Effective Pellet Volume Expansion	17
Figure 11: 1D Steady State Axial Temperatures	20
Figure 12: Steady State Axial Temperatures	20
Figure 13: Steady State Radial Temperatures	21
Figure 14: Oxidized Layer Model	22
Figure 15: Oxide Diffusion Limiting Model	22
Figure 16: Experimental Loop Setup	24
Figure 17: Pellet Surface Area vs. Loading	25
Figure 18: Oxygen Uptake of a Pellet at 800°C	26
Figure 19: 1D Predicted Temperatures within bed	31
Figure 20: Predicted Bed Temperatures	32
Figure 21: Predicted Wall Temperatures	33
Figure 22: Predicted Oxygen Absorption	33
Figure 23: Experimental Internal Temperatures	34
Figure 24: Experimental External Temperatures	35
Figure 25: Getter Bed after Air-Ingress	35
Figure 26: Oxygen Breakthrough Comparison	36
Figure 27: Axisymmetric TC 0 and TC1 Comparison	37
Figure 28: Axisymmetric TC 2 Comparison	37
Figure 29: Axisymmetric TC 3 Comparison	38
Figure 30: Axisymmetric TC 4 Comparison	38
Figure 31: Axisymmetric Wall Temperature Comparison	39
Figure A1: Pressure Decrease from 1 Pellet at 800°C	44
Figure A2: Mass Spectrometer Normalized Output, 800°C	44
Figure A3: Stagnant Experimental Setup	46
Figure A4: Stagnant Experimental Pressure	47
Figure B1: Air Density Variation with Temperature	49
Figure B2: Air Specific Heat Variation with Temperature	50
Figure B3: Air Viscosity Variation with Temperature	50
Figure B4: Air Thermal Conductivity Variation with Temperature	51
Figure C1: Metal Specific Heat Temperature Variation	54
Figure D1: Stainless Steel Temperature and Surface Condition Emissivity Variation	55
Table A1: Experimental Curve Fits	43
Table A2: Stagnant Experimental Results	47
Table C1: Constants for Oxidation of Zr, Fe, and Mn	52
Table C2: Property Characteristics of Zr, Fe, Mn, and Al	53
Table C3: Specific Heat Temperature Variation Parameters	53
Table D1: Stainless Steel Emissivity Temperature Variation	55
Table E1: Axisymmetric Node Temperatures and Masses	57

Chapter 1 INTRODUCTION

In order to maintain safe tritium handling practices, gas cleanup loops are used to ensure that no radioactive tritium is released up an exhaust stack. The loop normally contains a series of metallic getter beds that remove various impurities from the gas stream and then absorb the tritium itself. Figure 1 shows an example flow loop.

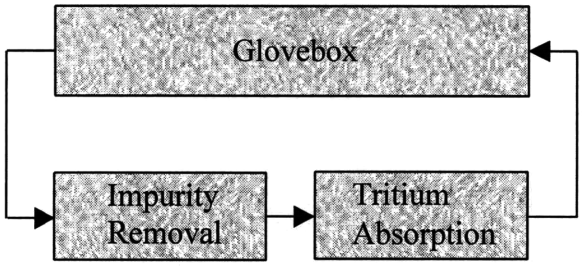

Figure 1: Glovebox Flow Loop

Many metals have been evaluated for the sorption of hydrogen isotopes, particularly tritium. The sorption technology covers a broad range of applications including nuclear fusion, hydrogen isotope chemical compression, and tritium handling, purification, and storage. Uranium beds have been thoroughly studied and are widely employed as metal tritide interim storage devices. However, due to the high chemical reactivity and restrictive use of nuclear materials, alternative getters such as vanadium, lanthanum, ytrium, titanium, and zirconium in pure and alloy forms are also of interest (Baker, 1993).

Independent of which metal alloy is employed for collection and storage of tritium, the influence of reactive impurities on getter performance is critical. The most important impurities found in various tritium systems are O_2, CO, CO_2, N_2, NQ_3, CQ_4, and Q_2O (Q=H, D, or T). All of the candidate metals and metal alloys irreversibly retain some part of the reaction products of these gaseous impurities which adversely affects their performance (Baker, 1993).

Since both tritium absorption and desorption kinetics and capacity are degraded as the oxygen content increases in the getter, it is desirable to purify the input stream before it reaches the tritium collecting bed. One such impurity removal bed used in the Tritium Science and Engineering group at Los Alamos National Laboratory is a zirconium-manganese-iron alloy (commercially available SAES St-909) bed. The most significant reaction within this St-909 getter bed is the highly exothermic oxidation of the pellets. In normal operation, the ZrMnFe (St-909) pellets within the getter bed remove a small amount of oxygen from the input gas stream. In the event of an equipment failure, human error, or accident within the glovebox flow loop, tubes could be cut, broken, or damaged and allow room air to be forced to flow through the system. During this unexpected inrush of air into the system, extreme temperatures could be reached that would cause the getter bed to fail. Also, since the objective of the St-909 bed is to remove impurities, namely oxygen, from the gas stream, the oxygen load and breakthrough performance of the bed under air-ingress conditions was of concern. The thermal transient response and the oxygen breakthrough profile of a St-909 getter bed were therefore desired under the failure mode of an air-ingress.

1.1 Overview

A St-909 getter bed contains metal pellets that are short cylinders, each with a 6 mm diameter, 4 mm thickness, and a mass of 0.6 g. The St-909 pellets are composed of 40.5% zirconium, 25% iron, 24.5% manganese, and 10% aluminum. A single pellet, fully oxidized with 0.259 g O_2, releases almost 4 kJ of heat. At a constant temperature, a pellet typically completes its reaction within 3-4 hours. About 2300 pellets weighing 1.4 kg total are packed into a cylindrical bed that is 6.5 cm in diameter and 20 cm in length.

A line rupture somewhere in the gas flow loop of a glovebox cleanup system would subject the pellets to out-of-design oxygen input. Normally the bed sees less than 1% oxygen, versus the 20% oxygen input the bed would experience in air. The goal is to understand the oxidation reaction and bed behavior processes, and finally to determine the structural response of the primary bed container.

The models presented here describe the oxidation reaction mathematically, including the temperature dependence of the oxide diffusivity into the pellet and swelling of the pellets, and the temperatures of the solid and fluid at discrete points throughout the bed. To confirm the models, both small-scale experiments on the pellets and a full-scale air-ingress experiment on the getter bed were conducted.

1.2 Experimental Setup

The full-scale experimental setup included a production size (20 cm x 7 cm diameter) St-909 bed surrounded by a coil heater, a heat shield, a preheater, and then an outer vacuum shell. This is shown in Figure 2. The containers were all made from 304L stainless steel.

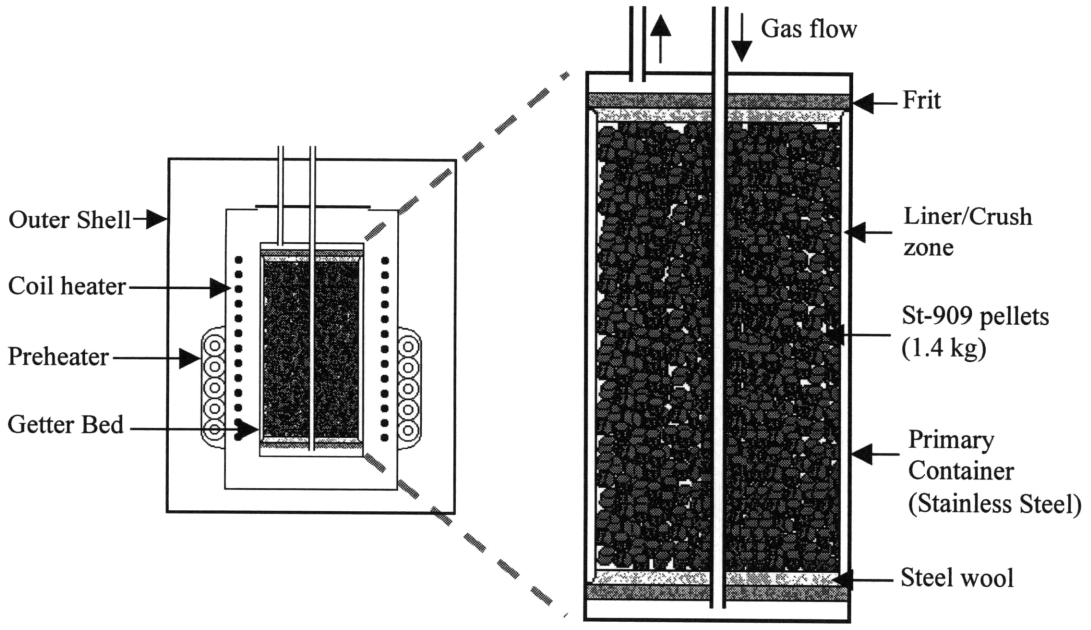

Figure 2: Getter Bed System

The right half of Figure 2 shows the detail of the St-909 getter bed. On the top and on the bottom were porous metal frits that restrained the pellets. The gas flowed down a center tube and then flowed upwards and exited at the top of the bed. As the pellets reacted with oxygen, they swelled and could actually double in volume when fully loaded. To allow for some of this expansion, extra space was provided in both the radial and axial directions. In the axial direction, about 1.25 cm (0.5 in.) of steel wool was placed in the bottom of the bed. In the radial direction, a crush zone was created with a liner. The liner diameter was initially 5.95 cm (2.34 in.) which could expand freely up to the inner 7 cm (2.75 in.) diameter of the primary container.

A coil heater surrounded the getter bed in order to raise it to its normal operating temperature of 650°C. The resistance heater had an available 2400W at 240V AC, though because these power levels were not required, the heater ran at 140V. A regenerative preheater used the bed exit flow to heat the gas before it entered the bed. The preheater would typically heat the gas from ambient temperature up to 400°C before it entered the top of the bed, and after passing through the center tube of the bed and the bottom frit, the gas would reach 600°C. Within the outer shell, a vacuum of less than 10^{-4} Pa (10^{-6} torr) was held using a turbomolecular pump.

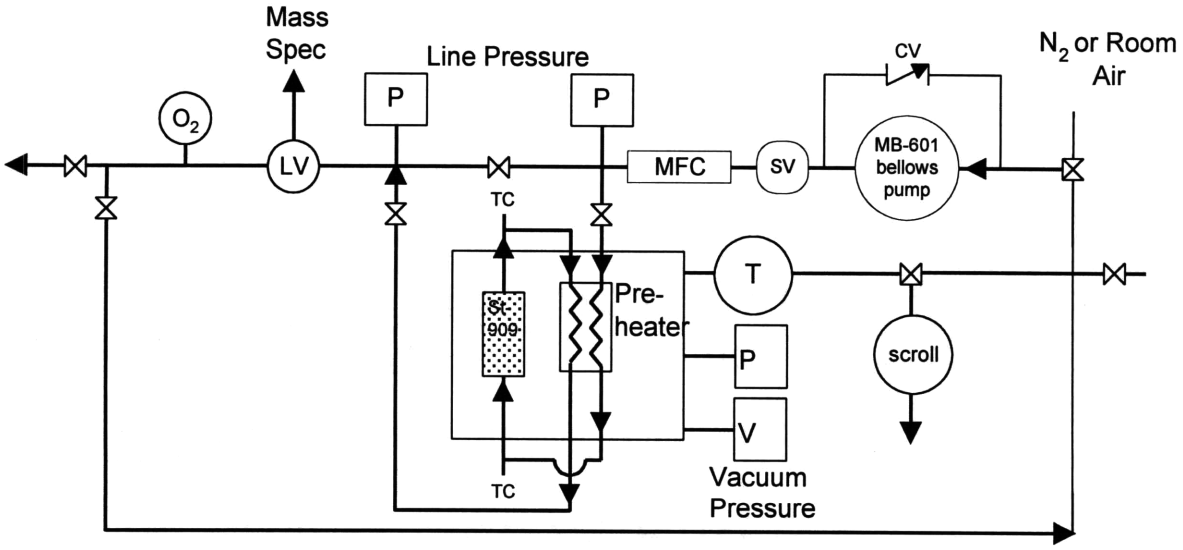

V - Granville Phillips Nude Ion Gauge
P - 1000 torr Baratron
O_2 - Nyad Oxygen Monitor
LV - Varian flow through leak valve
T - Varian V70 turbo/drag pump
MFC - MKS 200 slm range mass flow controller
CV - 25psig check valve
SV - 1 liter surge volume

Figure 3: Schematic of Full-Scale Experiment

Figure 3 shows a schematic diagram of the full-scale experimental setup. The flow through the bed was set as either pure nitrogen, as it would experience in normal getter bed operations, or room air, as it experienced under air-ingress failure conditions. A metal bellows pump forced gas through the bed with an average pressure drop across the bed of 13.3 kPa (100 torr or 2 psi). The mass flow controller kept the flow in the air-

ingress experiment at 0.00025 m^3/s (15 slm), the flow rate at which the glovebox normally operated based on a reasonable system purification time and desired residency rates within the getter beds. Finally, both a quadrupole mass spectrometer and a Nyad (model 232) oxygen sensor measured the oxygen coming out of the bed.

Figure 4 shows two photos of the full-scale experimental setup.

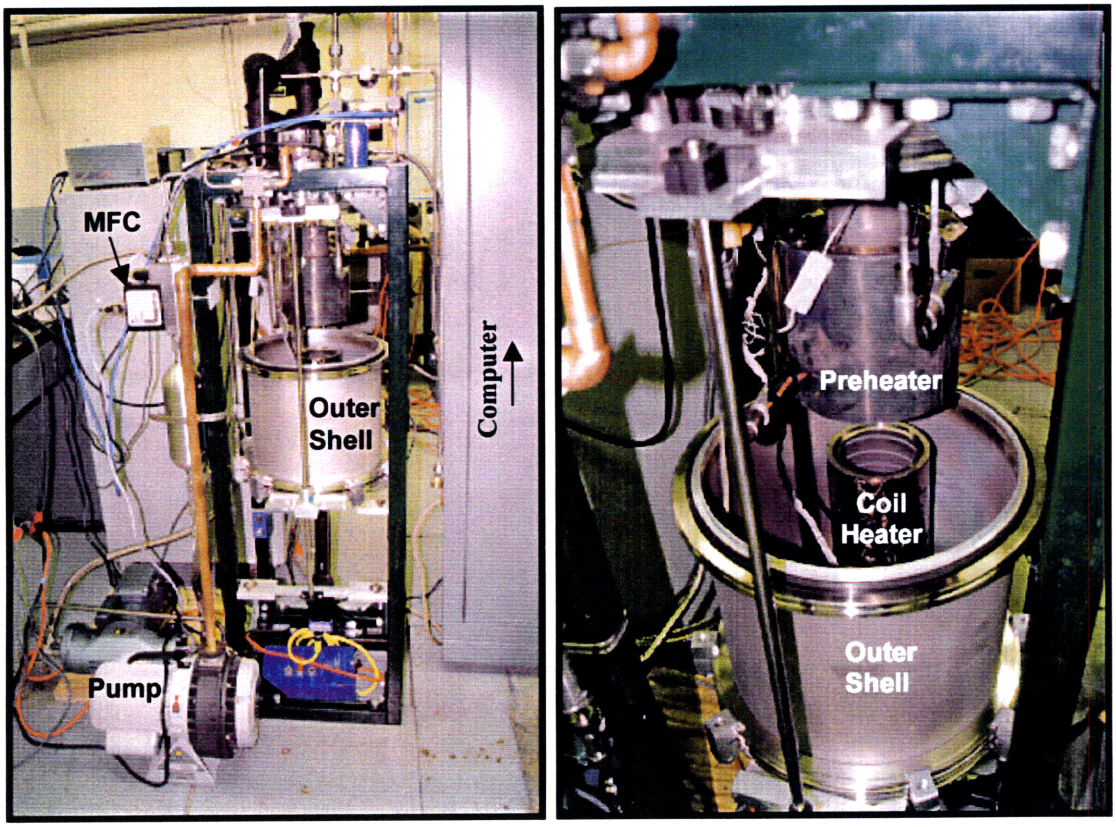

Figure 4: Full-Scale Experimental Setup

The photo on the left shows the larger system including pumps, tubing, pressure gauges, and wiring. The labeled pump was the Edward's ESDP12 high vacuum pump. The metal bellows pump behind the turbo pump was from Senior Flexonics, Inc. (MB-601Mod). The mass flow controller was from MKS Instruments. On the right and left of the setup were the locations for the computers for data acquisition before and during the experiment. National Instrument's Labview was used to collect thermocouple measurements, pressure data, flow rate and oxygen sensor percentages. Quadstar collected the residual gas analyzer data from the Balzar's QM421 Quadrupole Mass Spectrometer. The photo on the right side of Figure 4 shows a close up view of an open system. The outer shell was lowered about 45 cm (18 in.) to gain access to the inner cylinders.

Chapter 2 MODELS OF ST-909 BED

2.1 Fundamental Equations Describing Solid and Fluid Temperatures

The theoretical analysis of the bed began with the generation of fundamental equations describing the bed temperatures. Taking a differential control volume, or a slice through the bed, perpendicular to the fluid flow allowed generation of two partial differential equations describing the fluid and solid temperatures within the bed. Within the differential control volume, heat was transferred via axial conduction, convection from the pellet to the fluid, and airflow as indicated in Figure 5. Radiation within the bed was only considered indirectly through the effective thermal conductivity of the bed. This was a one dimensional, or axial view of a getter bed.

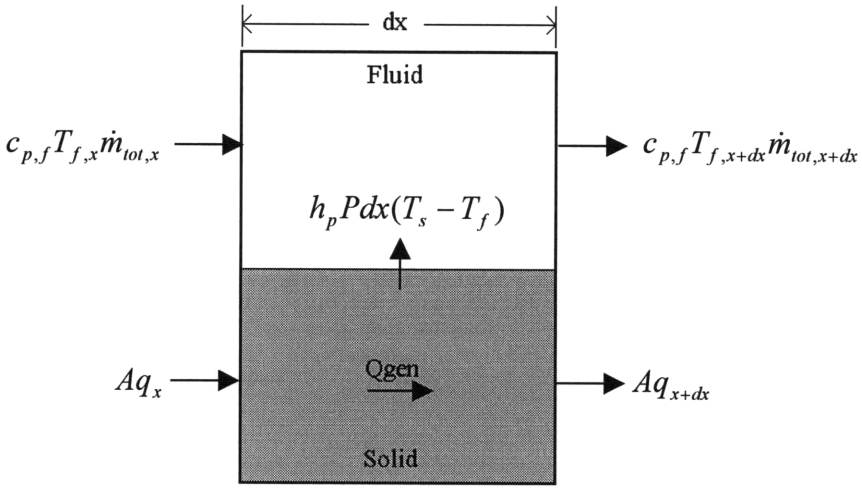

Figure 5: 1-D Differential Control Volume

Balancing the heat flows shown in Figure 5 yielded the following two partial differential equations:

$$k_s A_c \frac{\partial^2 T_s}{\partial x^2} - h_p P(T_s - T_f) + \widetilde{C}\frac{\partial(\dot{m}_{O2})}{\partial x} = (1-\varepsilon_b)\rho_s A_c c_{p,s}\frac{\partial T_s}{\partial t} \quad (1)$$

$$c_{p,f}\frac{\partial(\dot{m}_{tot}T_f)}{\partial x} + h_p P(T_f - T_s) = -\varepsilon_b \rho_f A_c c_{p,f}\frac{\partial T_f}{\partial t} \quad (2)$$

where k_s is the solid conductivity, A_c is the bed cross sectional area, h_p is the heat transfer coefficient, P is the transfer perimeter, $\widetilde{C}$ is a newly defined constant relating the heat generation and amount of material oxidized, ε_b is the void fraction within the bed, ρ is the density, c_p is the specific heat, $\dot{m}$ is the mass flow rate, and T is temperature. A complete list of nomenclature can be found following Chapter 6. The boundary conditions on the model consisted of the following: thermal radiation radially to a fixed temperature sink as the bed was enclosed in a vacuum, a prescribed inlet temperature, and an exiting heat flux at the end of the bed as the fluid carried heat out of the bed. Further explanation of the boundary conditions can be found in Section 2.5.

Extending this procedure into an axisymmetric view of the getter bed yielded the following two equations, where radial conduction was considered:

$$k_{eff} A_c \left[\frac{\partial^2 T_s}{\partial x^2} + \frac{1}{r} \frac{\partial}{\partial r} \left(r \frac{\partial T_s}{\partial r} \right) \right] - h_p P (T_s - T_f) + \tilde{C} \frac{\partial (\dot{m}_{O2})}{\partial x} = (1 - \varepsilon_b) \rho_s A_c c_{p,s} \frac{\partial T_s}{\partial t} \quad (3)$$

$$c_{p,f} \frac{\partial (\dot{m}_{tot} T_f)}{\partial x} + h_p P (T_f - T_s) = -\varepsilon_b \rho_f A_c c_{p,f} \frac{\partial T_f}{\partial t} \quad (4)$$

The unknowns in the above equations were the temperatures of the solid, T_s, and the fluid, T_f, as well as the mass flow of oxygen into the pellets, $\dot{m}_{O2}$. This last unknown was difficult to characterize and a simple equation to describe its behavior did not exist. The heat generated within the bed depended on the flow of oxygen into the pellet. The oxidation rate also increased with temperature and depended on the amount of material already oxidized. The oxygen within the pellet needed to be solved for iteratively, stepping through time. Therefore, to solve for the temperature distribution within the bed, a finite difference approach was used.

2.2 One Dimensional Finite Difference Model

As an alternative to solving the coupled set of partial differential equations, a one dimensional finite difference model was used. The model was later extended into an axisymmetric model of the bed, but for simplicity the one-dimensional model is first introduced. The 1D model divided up the getter bed into 50 sections, each with a thickness Δl, as shown in Figure 6. A sample slice and its corresponding heat transfer paths can be seen in Figure 7. The fluid was at a temperature of T_i and the solid temperature was T_{50+i}.

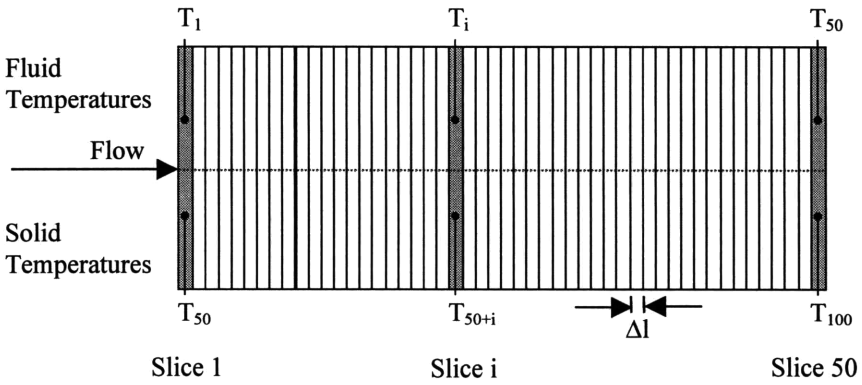

Figure 6: Getter Bed in 50 Slices

The various modes of heat transfer in the finite difference model included conduction through the pellets, convection between the pellets and the air flowing through the bed, and radiation from the bed to its surroundings. Heat was also transferred by flowing air, and generated by the exothermic oxidation reaction of air with the pellets.

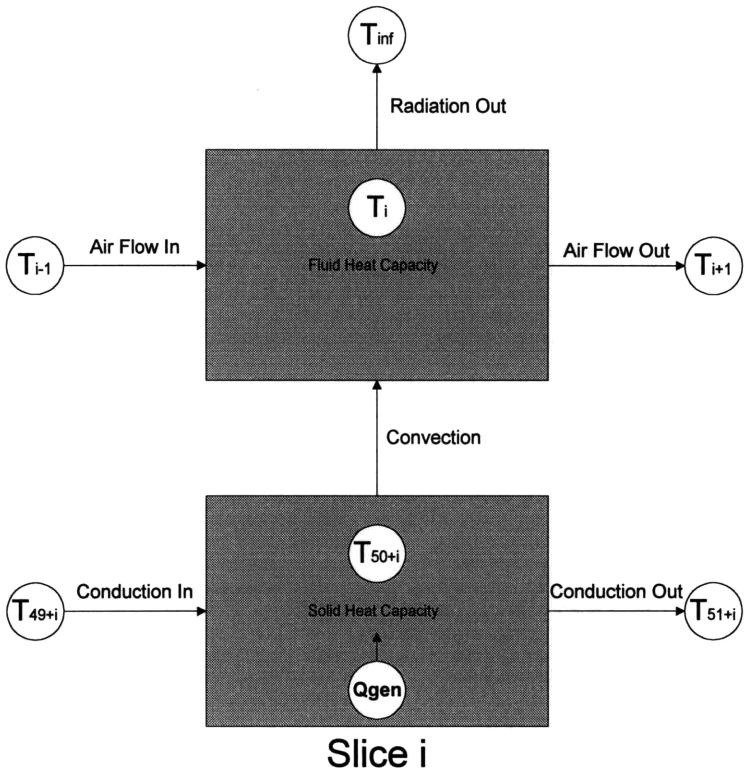

Figure 7: 1D Finite Difference Model

From the first law of thermodynamics, the energy stored in a slice must equal the energy generated plus the energy coming into the boundary minus the energy leaving the boundary. For the boundaries given by the shaded boxes in Figure 7, the first law of thermodynamics gave the following:

$$Q_{stored} = Q_{gen} + Q_{in} - Q_{out} \tag{5}$$

$$Fluid_{HeatCap} = Conv_{in} + AirFlow_{in} - AirFlow_{out} - Rad_{out} \tag{6}$$

$$Solid_{HeatCap} = Q_{gen} + Cond_{in} - Cond_{out} - Conv_{out} \tag{7}$$

2.2.1 Fluid Control Volume

For the fluid section heat balance, the terms from Equation 6 were as follows. The heat capacity associated with the fluid was given by:

$$Fluid_{HeatCap} = \Delta l \varepsilon_b \rho_f A_c c_{p,f} \frac{\partial T_i}{\partial t} \equiv C_1 \frac{\partial T_i}{\partial t} \tag{8}$$

where ρ_f is the density of the fluid, $c_{p,f}$ is the heat capacity of the fluid, and T_i is the temperature of the fluid at slice i. Both the density and heat capacity variation with temperature can be found in Appendix B.

Convection between the pellets and the fluid varied with the heat transfer coefficient, which in turn depended on the fluid viscosity, fluid mass flow rate, and characteristic dimensions of the bed and pellets. The convection term was given by the following (Mills, 1995):

$$Conv_{out} = h_p P \Delta l (T_{50+i} - T_i) = Conv_{in} \equiv C_2 (T_{50+i} - T_i) \tag{9}$$

$$\left.\begin{aligned} P &= aA_c = \frac{A_p}{V_p}(1-\varepsilon_b)A_c \\ h_p &= \frac{k_f}{L}(.5\,\mathrm{Re}^{1/2} + .2\,\mathrm{Re}^{2/3})\,\mathrm{Pr}^{1/3} \\ \mathrm{Re} &= \frac{VL\rho_f}{\mu_f} = \frac{(\frac{6\varepsilon b}{a})\dot{m}_{left}}{\mu_f \varepsilon_b A_c} \end{aligned}\right\} \tag{10}$$

where P is the heat transfer perimeter, a is the total surface area of particles per bed volume, A_p is the surface area of a pellet, V_p is the volume of a pellet, h_p is the heat transfer coefficient, Re is the Reynolds number associated with packed bed flow, Pr is the Prandtl number, V is velocity, L is a characteristic length of the bed, μ_f is the fluid viscosity, and $\dot{m}_{left}$ is the mass flow rate defined by Equation 12. Note that the fluid density, viscosity, and conductivity vary with temperature, as given in Appendix B. The heat transfer coefficient behavior described by Equation 10 was valid over a Reynolds number range from 20 to 7600. However, the flow within the St-909 getter bed was very low and the Reynolds number was about 5. When the Reynolds number got this low, the Nusselt number had a tendency to approach a constant, as shown by Achenbach (1995). The Nusselt number value at low Reynolds number was close to that predicted at the lower bound of the above equation, therefore the low Reynolds number behavior within the bed was approximated by using Equation 10 at its lower bound.

The flow of air through the bed carried energy across the fluid boundary. Since oxygen was absorbed from the air stream as it passed through the bed, the mass flow rate through the bed correspondingly decreased, as shown in Equations 12 and 14. The two air flow terms were given by:

$$AirFlow_{in} = \dot{m}_{left} c_{p,f} (T_{i-1} - T_i) \equiv C_3 (T_{i-1} - T_i) \tag{11}$$

$$\dot{m}_{left} = \dot{m}_{tot} - \sum_{n=1}^{i-1} \frac{M_{n,t} - M_{n,t-\Delta t}}{\Delta t} \tag{12}$$

$$AirFlow_{out} = \dot{m}_{right} c_{p,f} (T_i - T_{i+1}) \equiv C_4 (T_i - T_{i+1}) \tag{13}$$

$$\dot{m}_{right} = \dot{m}_{tot} - \sum_{n=1}^{i} \frac{M_{n,t} - M_{n,t-\Delta t}}{\Delta t} \tag{14}$$

where $\dot{m}_{left}$ is the mass flow rate of air coming into slice i, $M_{n,t}$ is the mass of oxygen absorbed by the pellets in slice n at time t.

The fluid is in direct contact with the getter bed container. Therefore, the temperature of the bed that radiates outward is the fluid temperature. The radiative heat transfer was linearized around a mean temperature, T_{mean}, in order to simplify the analysis. The boundary condition chosen was that of radiation to a coil heater at 670°C. The radiation term was given by:

$$Rad_{out} = \frac{A_{surf}}{50}\sigma\varepsilon_{12}4T_{mean}^3(T_i - T_{inf}) \equiv C_9(T_i - T_{inf}) \tag{15}$$

$$\varepsilon_{12} = \frac{1}{1/\varepsilon_1 + A_1/A_2(1/\varepsilon_2 - 1)} \tag{16}$$

where A_{surf} is the total outer surface area of the getter bed, σ is the Stephan-Boltzmann constant, ε_{12} is the effective emissivity between two concentric cylinders, ε_i and A_i are the respective emissivity and surface area of surface i, and T_{inf} is the coil heater temperature.

2.2.2 Solid Control Volume

For the solid pellet section, each term from Equation 7 was defined as follows. The convection term was the same as given in Equation 10. The heat capacity associated with the pellets themselves was defined by:

$$Solid_{HeatCap} = \Delta l(1-\varepsilon_b)\rho_s A_c c_{p,s}\frac{\partial T_{50+i}}{\partial t} \equiv C_5\frac{\partial T_{50+i}}{\partial t} \tag{17}$$

where ε_b is the void fraction of the bed, ρ_s is the solid density, A_c is the cross sectional area of the bed, $c_{p,s}$ is the specific heat of the pellets, and T_{50+i} is the solid temperature at slice i.

Heat generation within a pellet slice varied with the mass uptake of oxygen because of the exothermic oxidation reaction. The generation term was given by:

$$\left.\begin{aligned} Q_{gen} &= \tilde{C} * n(M_t - M_{t-\Delta t}) \equiv C_6 \\ Q_{gen} &= 10.3 * n(\Delta H^\circ_{Zr} + \Delta H^\circ_{Mn} + \Delta H^\circ_{Fe})(M_t - M_{t-\Delta t}) \end{aligned}\right\} \tag{18}$$

$$\Delta H^\circ = A - CT/\ln(10) \tag{19}$$

where n is the number of pellets, M_t is the mass of oxidized oxygen within a single pellet at time t, ΔH° is the enthalpy of formation of the oxide [J/mol], and A and C are constants which depend on the material oxidizing, e.g. Zr, Mn, or Fe. There were 46 pellets per slice releasing heat. The derivation of $\tilde{C}$ and the values for A and C can be found in Appendix C.

For the one-dimensional model, conduction through the pellets depended on an effective axial thermal conductivity. This effective conductivity, k_{eff}, was determined both by the

conductivity of the fluid and the conductivity of the pellets. The conduction terms were given by (Wakao, 1982):

$$Cond_{in} = \frac{k_{eff} A_c}{\Delta l}(T_{49+i} - T_{50+i}) \equiv C_7(T_{49+i} - T_{50+i}) \tag{20}$$

$$Cond_{out} = \frac{k_{eff} A_c}{\Delta l}(T_{50+i} - T_{51+i}) \equiv C_8(T_{50+i} - T_{51+i}) \tag{21}$$

$$\left.\begin{aligned} k_{eff} &= k_f \left(\frac{k_s}{k_f}\right)^n \\ n &= .28 - .757 \log \varepsilon_b - .057 \log \frac{k_s}{k_f} \end{aligned}\right\} \tag{22}$$

where k_s is the conductivity of the solid pellets and k_f is the conductivity of the fluid. The fluid conductivity varied with temperature, as can be found in Appendix B.

2.3 Axisymmetric Model

One of the main concerns in the air-ingress scenario was the temperature of the primary container of the getter bed. It was not sufficient to have only an average temperature across a radial section of the bed, therefore an axisymmetric model was generated, as shown in Figure 8. This model of the bed expanded upon the 1D model to contain 50 axial slices and 7 radial sections.

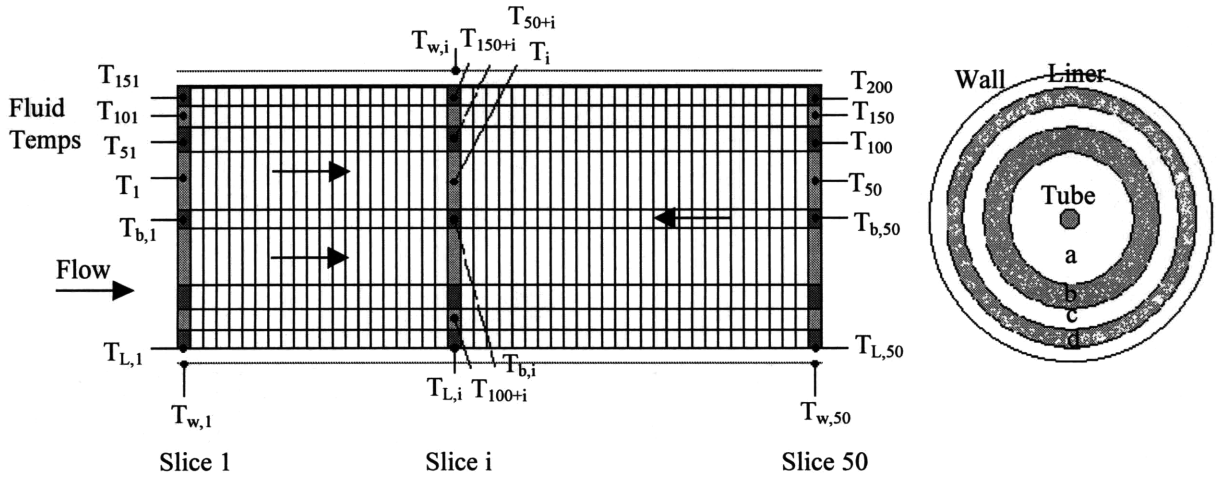

Figure 8: Getter Bed in Axial and Radial Sections

The different radial temperatures were for the inlet gas at the center of the bed, four inner sections within the bed, a liner temperature node, and finally the wall temperature. The four inner radial sections, labeled a-d in Figure 8, were chosen to have equal cross sectional areas. The temperatures labeled T shown in Figure 8 are the fluid temperatures. The corresponding solid temperatures were indexed 200 above the fluid indices. Further explanation of the temperature indices can be found in Appendix E.

Figure 9 shows a schematic diagram of a slice i from the axisymmetric model. The added heat transfer modes in comparison to the 1D model included convection to the inlet gas flowing through the center tube, radial conduction through the solid, wall convection from the fluid to the liner, and radiation from the liner to the wall.

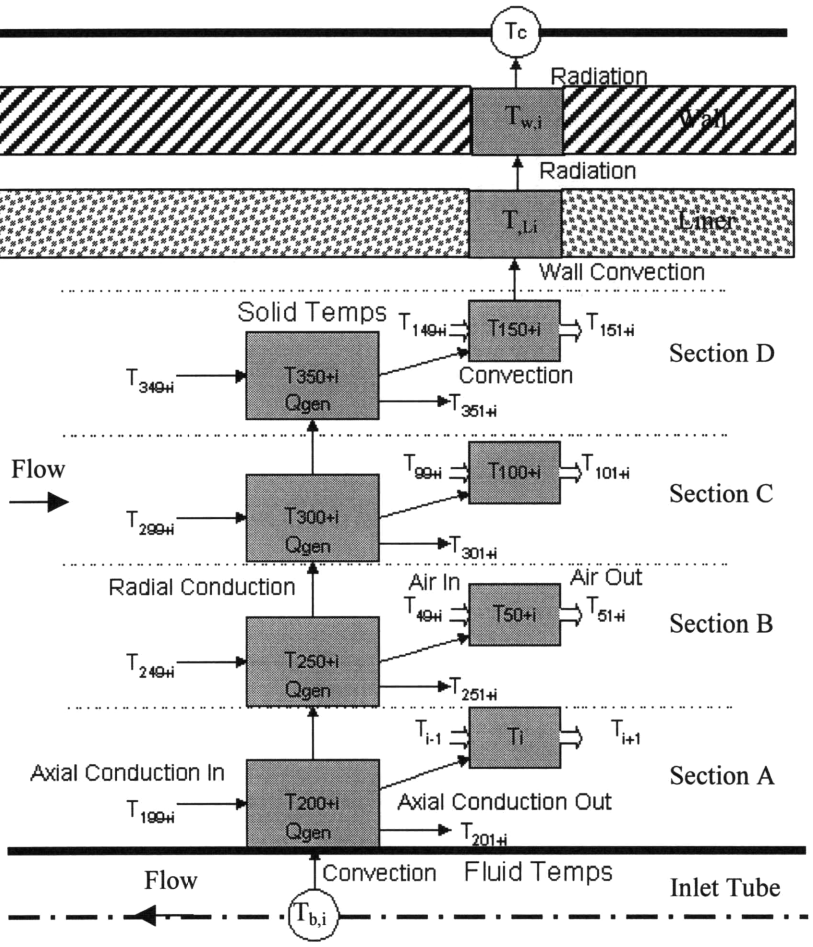

Figure 9: Axisymmetric Finite Difference Model

This axisymmetric model had 50 inlet gas temperature nodes, 200 fluid temperature nodes, 200 solid temperature nodes, 50 liner temperature nodes and 50 wall temperature nodes. The coefficients described above in the 1D model were the same in this model, with the only change being that the cross sectional area in Equations 8-21 was divided by four, and the number of pellets per section became 11.5 instead of 46. The new terms in the axisymmetric model are described below.

The gas entered the top of the bed at a temperature near 400°C after being heated by the preheater. The walls of the inlet tube then heated up the gas. Using relations for laminar tube flow, the bulk temperature of the fluid, T_b, was described by the following relation:

$$\frac{T_{b,i} - T_w}{T_{b,init} - T_w} = \exp\left(\frac{-xh\pi d_{tube}}{\dot{m}c_p}\right) \tag{23}$$

where x was the axial length into the bed. In the finite element model, x was equal to the slice length Δl and the initial bulk temperature was simply the temperature of the fluid at the previous slice. The inlet tube had an outer diameter of 6.35 mm (.25 in.) and a thickness of 1 mm (.0394 in.). At the given 15 slm, the Reynolds number based on the diameter of the inlet tube was between 1100 and 1450 at either end of the tube. Both cases were below the turbulence transition Reynolds number of 2000, so that a laminar Nusselt number equal to a constant of 4.364 was used to calculate the heat transfer coefficient h. The convection from the inlet gas bulk temperature to the innermost radial section of the bed was described by the following:

$$Conv_{in} = h\pi d_{tube}\Delta l(T_{200+i} - T_{b,i}) \equiv C_{13}(T_{200+i} - T_{b,i}) \tag{24}$$

This convection term only transferred heat from the solid temperature within Section A of the getter bed to the inlet gas.

The pellet radial conduction varied with the given radial section. This conduction term was defined for a given section, say from b to c, by the following equation:

$$Cond_{rad} = \frac{k_{eff,r}2\pi\Delta l}{\ln(r_{outer}/r_{inner})}(T_{250+i} - T_{300+i}) \equiv C_{10}(T_{250+i} - T_{300+i}) \tag{25}$$

where the outer and inner radii were taken at the radial midpoint of the given section. For example, the temperature node of section b was at a radius of 2.1 cm—the midpoint of its boundaries of 1.746 cm and 2.47 cm. The temperature node of section c was at 2.75 cm —the midpoint of its boundaries of 2.47 cm and 3.025 cm. Therefore, for the radial conduction between section b and c, the outer radius was 2.75 cm and the inner radius was 2.1 cm.

The wall convection term from Section D to the liner was given by the following equation (Wakao, 1982):

$$Conv_{out} = h_w A_{outer}(T_{150+i} - T_{L,i}) \equiv C_{11}(T_{150+i} - T_{L,i}) \tag{26}$$

$$\left.\begin{aligned} h_w &= \frac{k_f}{d_p}0.16\,\mathrm{Re}^{0.93} \\ \mathrm{Re} &= \frac{d_p Q\rho_f}{A_c\mu_f} \end{aligned}\right\} \tag{27}$$

where the wall heat transfer coefficient, h_w, is defined by equation 27. The range of Reynolds numbers over which Equation 27 was valid was the same as the range for Equation 10 (20<Re<7600). The same assumptions were made about low Reynolds

number behavior (Achenbach, 1995) as before for Equation 10, which gave a heat transfer coefficient equal to that predicted by Equation 27 at its lower bound.

The liner then radiated to the wall of the primary container. This was maintained until the pellets swelled so much so that they pushed the liner out to the wall of the primary container, as is described below. This radiation was described by the following:

$$Rad_{out} = A\sigma\varepsilon_{12}4T_{mean}^3(T_{L,i} - T_{w,i}) \equiv C_{12}(T_{L,i} - T_{w,i}) \tag{28}$$

$$\varepsilon_{12} = \frac{1}{1/\varepsilon_1 + A_1/A_2(1/\varepsilon_2 - 1)} \tag{29}$$

which is similar to Equations 15 and 16, differing in the values of the parameters only. Again, the stainless steel emissivity varied with temperature. Once the swelling pushed the liner to the inner diameter of the primary container, the temperatures were assumed to be the same and the radiation term given in Equation 28 was ignored.

The swelling of the pellets and therefore a decrease in the void fraction within the bed was also incorporated into the axisymmetric model. Section 3.3 below describes how the pellet radius was found as a function of the mass of oxygen absorbed. Using this swelling data from small-scale experiments also gave relations for both the actual volume expansion and the effective volume expansion as a function of loading. Figure 10 shows the measured volume expansion of several pellets at various loadings. The effective volume expansion was obtained by measuring the pellet's final diameter and thickness, with cracks included. The actual volume expansion was obtained by subtracting the measured crack space from the effective volume.

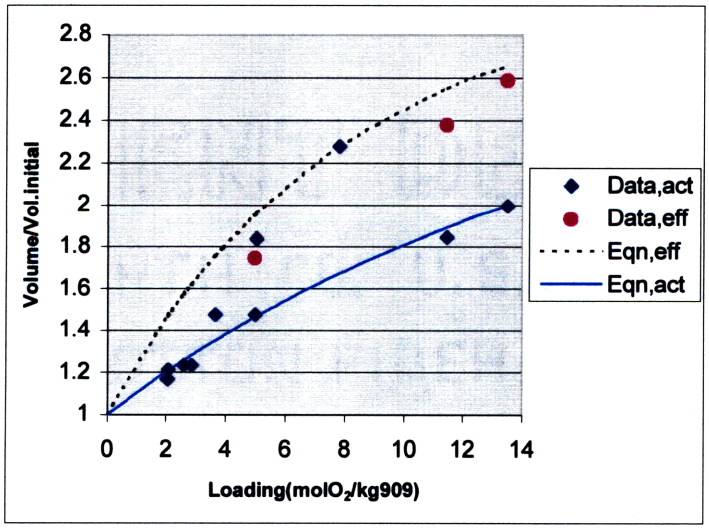

Figure 10: Actual and Effective Pellet Volume Expansion

Equations 30 and 31 describe the general behavior of the swelling shown in Figure 10.

$$Vol_{eff} = Vol_{p,init}\left(1 + 2\left(1 - \exp(-4468.75M_{O_2})\right)\right) \tag{30}$$

$$Vol_{act} = Vol_{p,init}\left(1 + 1.8\left(1 - \exp(-2062.5 M_{O_2})\right)\right) \tag{31}$$

where M_{O_2} is the mass of oxygen absorbed by the pellet.

The void fraction within the bed could be determined once the actual and effective volume of the pellets was known. It was calculated using the following equation:

$$e_b = \frac{Vol_{eff} - Vol_{act}}{Vol_{eff}} \tag{32}$$

The effective volume was equal to the initial available volume before the pellets had swelled enough to expand the liner.

2.4 Initial Conditions: Steady State Packed Bed Model

To determine the initial temperatures of the packed getter bed, a steady state solution with no exothermic reaction was used. A closed form solution to this problem was achievable because the solid and fluid temperatures were assumed to be the same and there was no heat generation within the bed. This steady state model was the analytical solution to the following partial differential equation (Wakao, 1982):

$$Gc_f \frac{\partial T}{\partial x} = k_{eff,r} \frac{1}{r} \frac{\partial}{\partial r}\left(r \frac{\partial T}{\partial r}\right) + k_{eff,ax} \frac{\partial^2 T}{\partial x^2} \tag{33}$$

where G is the fluid mass velocity per unit area of bed cross-section. Using separation of variables, the solution for Equation 33 was obtained. The infinite series solution converged rapidly, and the solution deep within a bed (x>0.6 cm), was given by the following (Wakao, 1982):

$$\frac{T_w - T}{T_w - T_o} = \frac{2J_o(a_1 r / R_B)\exp[-a_1 k_{eff,r} x / R_B (k_{eff,r} k_{eff,ax})^{0.5}]}{a_1[1 + (a_1 / B)^2] J_1(a_1)} \tag{34}$$

where R_B is the bed radius, T_0 is the inlet temperature and T_w is the wall temperature. This solution was based on a semi-infinite bed, a given inlet temperature, a symmetric radial distribution, and convection to a constant wall temperature.

The constant B was defined by:

$$B = \frac{h_w R_T}{k_{eff,r}} \tag{35}$$

The term a_1 was the first root of the following equation of Bessel functions (J_0 is a Bessel function of the first kind and zeroth-order, and J_1 is that of first kind and first order):

$$BJ_0(a_1) = a_1 J_1(a_1) \tag{36}$$

The wall heat transfer coefficient for a cylindrical particle-air system, h_w, was determined by the following (Wakao, 1982):

$$h_w = \frac{k_f}{d_p} 0.16 \,\mathrm{Re}^{0.93} \tag{37}$$

where the Reynolds number is based on the superficial fluid velocity, which the gas would have through a bed with no pellets, and the pellet diameter:

$$\mathrm{Re} = \frac{d_p Q \rho_f}{A_c \mu_f} \tag{38}$$

where Q is flow and d_p is the diameter of the pellet.

At 15 slm and 600°C, the conductivity of air was close to 0.06 W/mK and the conductivity of the solid getter material was approximately 40 W/mK. Equation 22 predicted an effective thermal conductivity near 1 W/mK. However, Equation 22 was based on spherical, and not cylindrical pellets. The actual thermal conductivity was therefore expected to be slightly higher than the prediction by the equation. The axial and radial thermal conductivities were increased until agreement between steady state temperatures from theory and experiment matched. This occurred when the conductivities both had a value of near 5 W/mK.

2.4.1 Steady State-Initial Temperatures

The steady state temperatures predicted by the above packed bed model were used for the one-dimensional model, as shown in Figure 11. The third and fourth thermocouple temperature measurements were initially assumed to increase in temperature, as was predicted in Figure 11. However, the experimental behavior during the air-ingress showed the thermocouples reacting in reverse order. The axisymmetric steady state temperatures, described below, showed that the inlet tube slightly cooled the latter sections of the bed, and that the highest steady state temperature measurement was actually thermocouple 3. The thermocouple 3 and 4 readings were therefore swapped. The error expected with the thermocouple measurements was ±0.89%, or ±5.8°C on a 650°C measurement. See Appendix A for uncertainty analysis.

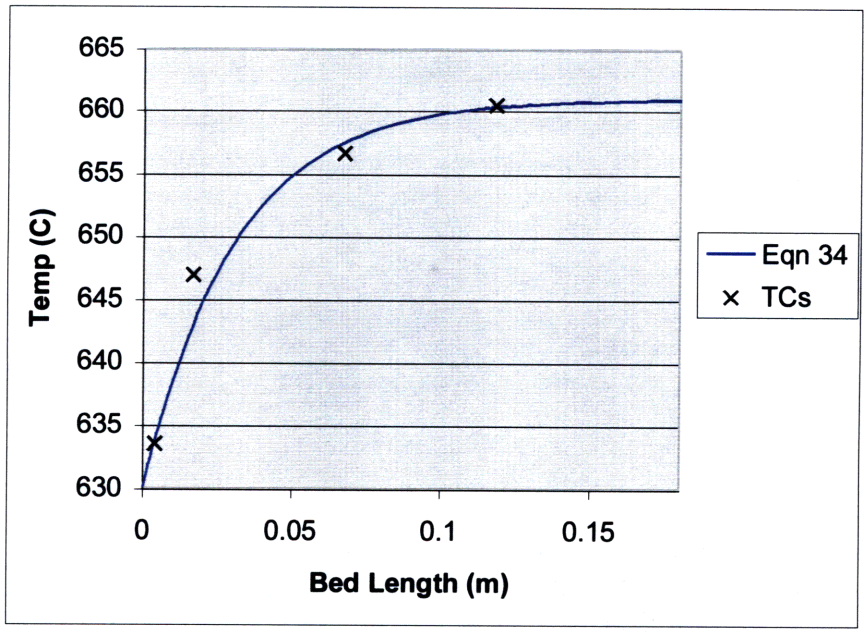

Figure 11: Closed Form Solution Steady State Axial Temperatures

The axisymmetric model, which included the inlet tube, liner, and wall temperatures, was run with no heat generation. Both the predicted axial steady state temperatures from the axisymmetric model and experimental thermocouple measurements are shown in Figure 12.

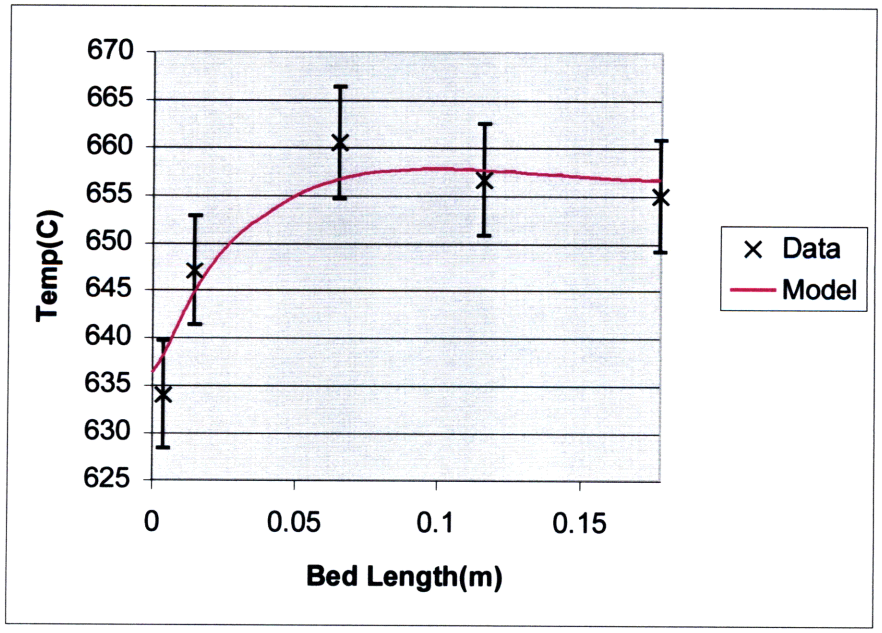

Figure 12: Steady State Axial Temperatures

The initial radial variation of temperature within the bed is shown to be small in Figure 13. The radial position of the thermocouples was at 1.59 cm (or .625 in.).

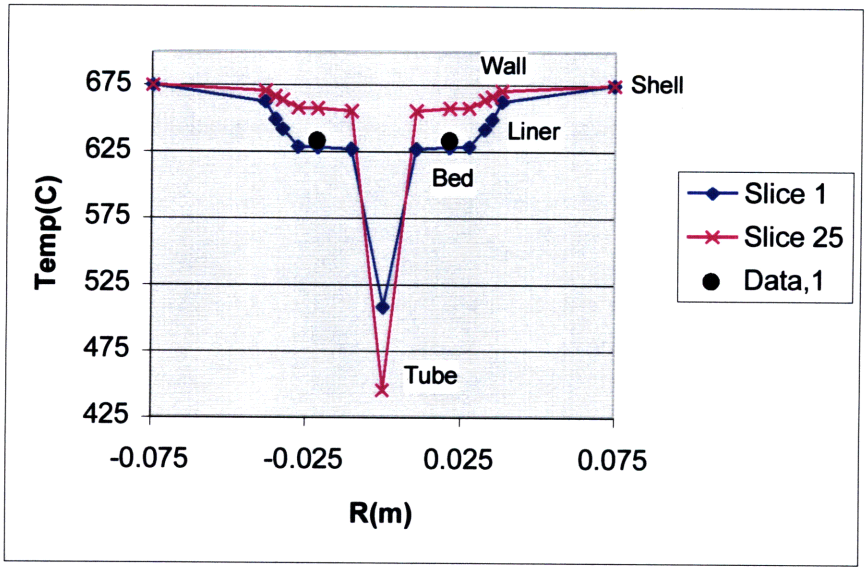

Figure 13: Steady State Radial Temperatures

2.5 Boundary Conditions

2.5.1 Axial—Inlet Fluid Temperature

The getter bed inlet air stream had to pass through the preheater before it entered the top of the bed. The temperature of the inlet gas in the test setup was 400°C, which was used as the gas inlet temperature for the axisymmetric model. The one-dimensional model did not account for heat transfer to the inlet tube and therefore used an inlet temperature at the bottom of the bed of 620°C, a steady state value determined experimentally by a thermocouple along the inlet gas tube. However, the inlet gas did tend to vary throughout the experiment.

2.5.2 Axial—Outlet Fluid Heat Transfer

The fluid exiting the bed carried heat away with it that was used to preheat the inlet gas. As an outlet boundary condition, this heat flux simply left the bed. This was used for both the 1D and axisymmetric models.

2.5.3 Radial—Radiation

The getter bed was enclosed in a vacuum that insulated it from excessive heat transfer and thereby reducing the required power for the coil heater during normal operations. Thus, for the one-dimensional model, the radiation term described by Equations 15-16 was the third boundary condition. For the axisymmetric model, the outer fluid element first transferred heat via convection to the liner, the liner radiated heat to the wall, and then the wall radiated heat to the heat shield. Both models eventually radiated to the heat shield that surrounded the coil heater, which was kept at a temperature of 670°C.

Chapter 3 OXIDE DIFFUSION LIMITING (ODL) MODEL FOR OXIDATION OF ST-909 PELLETS

The most significant variable that determined the temperature profile of the bed was the heat generated by the highly exothermic oxidation reaction of the pellets. One pellet reacted completely to a loading of 13.5 mol O_2/kg St-909 released around 4 kJ of energy. Some assumptions were made, as described below, in order to obtain an analytical expression for the pellet's mass uptake of oxygen as it varied with time.

Since the mechanism of the oxidation reaction was unknown, two different models were investigated as possible ways the oxide and oxygen were behaving. The first required that the fresh oxygen diffuse through a layer of oxidized metal before reaching unexposed pellet material, as shown in Figure 14. In this model, the oxidized layer (grey circles) remained stationary and unoxidized oxygen diffused through an ever-growing layer of oxidized pellet material. The second model required that the oxidized material itself diffuse into the pellet and leave a relatively fresh pellet surface for the oxygen to react with, as shown in Figure 15. The lines in Figure 15 show possible concentrations of oxidized material as it increased with time. This second model, called Oxide Diffusion Limiting Model, was more accurate and closely represented experimental measurements of the pellet's behavior.

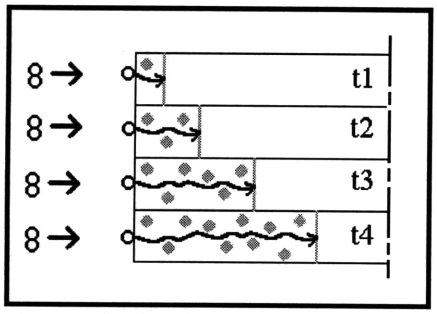

Figure 14: Oxidized Layer Model

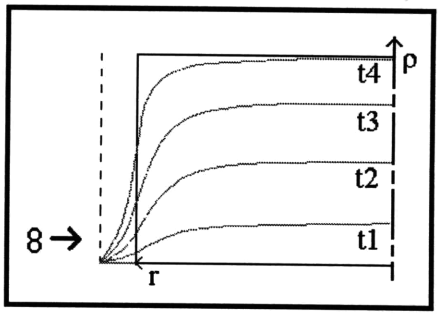

Figure 15: Oxide Diffusion Limiting Model

3.1 ODL Theoretical Solution

The Oxide Diffusion Limiting Model (ODL) was based on a particular solution to the mass diffusion equation. The pellet was assumed to be a sphere with oxygen diffusing into it from all surfaces. The surface density of the oxide was dependent on the amount of oxygen available to react with the pellet. The one dimensional mass diffusion equation in spherical coordinates was as follows (Poulikakos, 1994):

$$\frac{\partial \rho_{O_2}}{\partial t} = D_{eff} \frac{1}{r^2} \frac{\partial}{\partial r}\left(r^2 \frac{\partial \rho_{O_2}}{\partial r} \right) \tag{39}$$

where D_{eff} is an effective diffusivity of the metal oxide into the porous pellet, r is the radius, and ρ_{O_2} is the density of the oxide within the pellet. The solution to Equation 39, given a constant surface density was as follows (Welty, 1976):

$$\frac{\rho_{O2} - \rho_{surf}}{\rho_{init} - \rho_{surf}} = \frac{4}{\pi} \sum_{n=1,3}^{\infty} \frac{1}{n} \sin\left(\frac{n\pi(r + R_p)}{2R_p}\right) \exp\left(-\left(\frac{n\pi}{2}\right)^2 \frac{D_{eff} t}{R_p^2}\right) \quad (40)$$

where ρ_{surf} is the surface density, ρ_{init} is the initial density, and R_p is the radius of the pellet.

Only the overall mass uptake of oxygen was needed for the heat generation term. Therefore, to eliminate its radial variance, an average density was taken by finding the average value of ρ_{O_2}. Using the average density, the initial density, the surface density, and the volume of the pellet, the mass of oxygen within the pellet was found to be:

$$M_{O_2} = (M_{tot} - M_{init})\left[1 - \frac{4}{\pi^2} \sum_{n=1,3}^{\infty} \frac{2}{n^2} \exp\left(\left(\frac{-n\pi}{2}\right)^2 \frac{D_{eff} t}{R_p^2}\right)\right] \quad (41)$$

$$M_{tot} = volume(\rho_{surf} - \rho_{init}) \quad (42)$$

Equation 42 was used within the program to determine the oxygen within the pellet. It was therefore not required to know the surface density. Instead, the maximum oxygen mass varied throughout the bed. For slices that were more close to the end of the bed, this forcing mass was related to the oxygen percent reaching the particular slice.

The ODL model in its most simple form was an exponential mass uptake, dependent on the ratio of $D_{eff}(T)/R_p(oxidation)^2$. The pellets were porous with an 18% void space (free space divided by the volume) so that published values for an oxide diffusivity into a solid metal (Zr, Mn, or Fe) did not apply. Therefore, the temperature variation of the effective oxide diffusivity into the pellet needed to be experimentally determined by performing small-scale experiments on individual pellets.

3.2 Small-Scale Experiments

Several experiments were performed at LANL at temperatures ranging from 600-900°C. A single pellet was exposed to a closed system of air, and the pressure was measured as a function of time. At first, the experiment consisted of a stagnant volume of air reacting with the pellet, but the loadings achieved were only 15% ideal loading. See 'Additional Experimental Results' under Appendix A for a detailed description of initial tests. In order to increase the mass transfer coefficient to the pellet, a loop system with a pump was setup. This setup can be seen in Figure 16. The loadings achieved with the loop setup were much higher than initial test results and 100% ideal loading was accomplished during two experiments. A derivation of the definition of 100% ideal loading can be found in Appendix C.

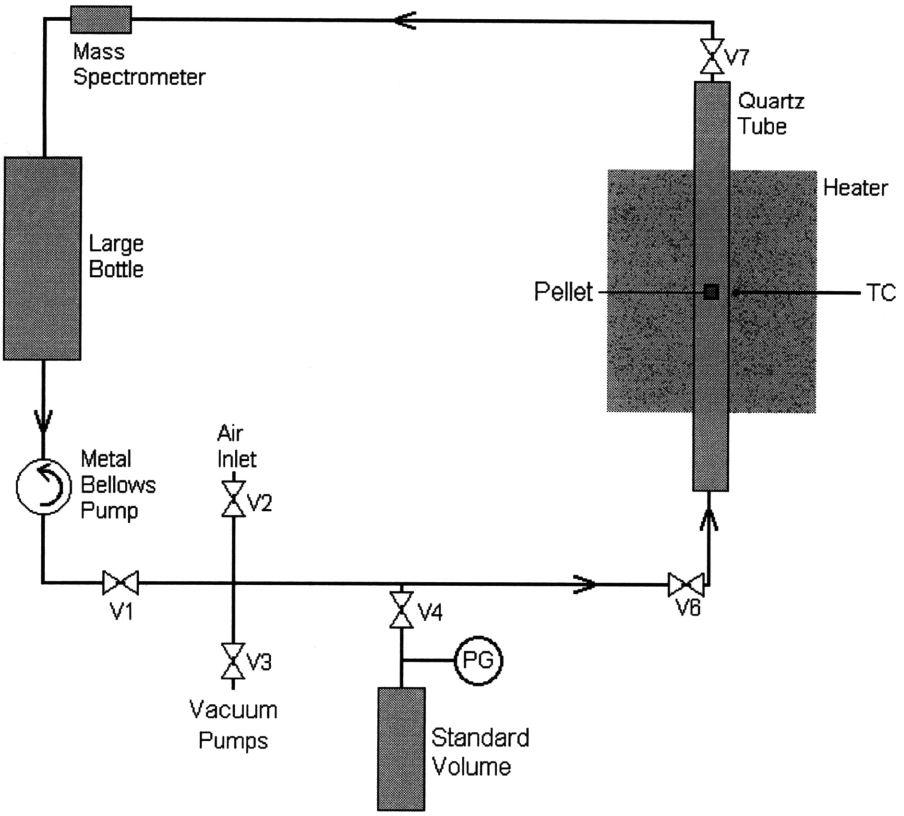

Figure 16: Experimental Loop Setup

The experimental procedure ran as follows:

1. Fittings greased around quartz tube with high vacuum grease.
2. Pumped entire volume down to below 0.66 Pa ($5x10^{-3}$ torr).
3. Raised temperature on quartz tube with heater to given set point (e.g. 600°C). Held under vacuum at high temperature for two hours to activate St-909 pellet.
4. Isolated quartz volume under vacuum (valve 6 and valve 7).
5. Cut off turbomolecular pump (valve 3).
6. Filled entire volume minus quartz volume (1379 cm^3) with air (valve 2).
7. Started Labview to record pressure and temperature of system. Started quadrupole mass spectrometer to record composition of gas within system.
8. Opened valve 6 (volume increases to 1590 cc). Started metal bellows pump. Labview captured pressure versus time response for system.
9. After reaching a pressure steady state, turned heater and bellows pump off and let cool.

The loadings achieved with this loop setup had a maximum of 13.5 mol O_2/kg St-909, corresponding to 100% ideal loading. Nitrogen loading of the pellets was a concern, but the mass spectrometer data showed that the nitrogen loading was minimal and did not significantly affect the oxygen loading capacity. A plot from the mass spectrometer data can be found in Appendix A under 'Mass Loading'.

3.3 Determination of Pellet Radius Variation

The variation of the pellet radius with absorbed oxygen needed to be determined before the theoretical model could be compared to the small-scale experimental results, thus giving the temperature variation of the effective oxide-pellet diffusivity.

When the St-909 pellets load with oxygen, they exhibit volume expansion. Experimentally, after loading reached about 40-60% of ideal, the pellets began to crack open. Based on measurements of pellets that were loaded from 15% up to 100% of ideal loading, a closely linear fit was found between available surface area to react with the oxygen and the loading. The loaded surface area was calculated by measuring the diameter and thickness of the loaded pellet if no cracking occurred. If the pellet cracked open some, the crack was measured and the additional surface area was summed with the swelled surface area. This pellet swelling can be seen in Figure 17 where the pellets that cracked open are distinguished from those that simply swelled.

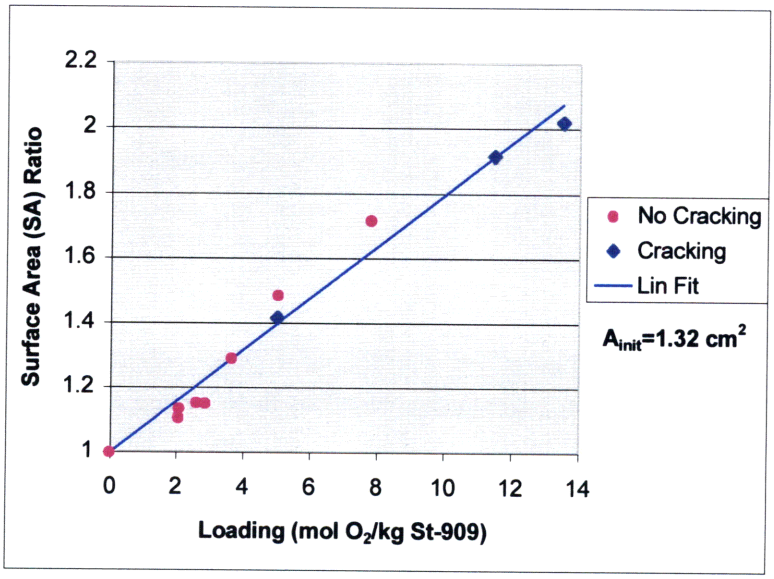

Figure 17: Pellet Surface Area vs. Loading

As the loading, or amount oxidized, increased, the surface area of a pellet was determined by using the linear fit from Figure 17 that followed Equation 37. By assuming that the ratio of the thickness of the pellet to the radius remains constant, the surface area was defined by Equation 38. These led to Equation 39, which described the dependence of the pellet radius on the oxygen already absorbed by the pellet.

$$SA = SA_{init}(1 + .002492 * load(g/mol)) \tag{43}$$

$$SA = 2\pi R_p^2 + 2\pi R_p(\frac{4}{3}R_p) \tag{44}$$

$$Rp = \left[\frac{SA_{init}}{4.666\pi}(1 + 4153.33M_t(kg))\right]^{0.5} \tag{45}$$

Equation 39 predicted that the radius could increase from 3 mm to 7.2 mm at maximum loading (2.4 times the original radius).

The effect of the swelling was an increase in the radius of the pellet, which decreased the ratio D_{eff}/R_p^2 on which the oxidation reaction rate was dependent. This swelling caused the oxidation reaction to occur more quickly on a fresh pellet and slow down as loading approached the full 13.5 mol O_2/kg St-909. The swelling also caused a need for the oxygen mass within the pellet to be solved for in an iterative fashion, marching through time. The initial oxygen uptake rate was determined for a given radius, the radius was then evaluated at that given mass oxidation, and this cycle would continue through time until full oxidation was achieved.

3.4 ODL Model Comparison to Experiments

The effective diffusivity of a St-909 pellet for a given temperature was determined by trial and comparison. For a given effective diffusivity, the ODL model predicted the time behavior of the oxidation, which was then compared to experimental values. An example of a comparison between the experimental values and predictions from the equation can be found in Figure 18. Experimental pressure curves for multiple experiments can be found in Appendix A.

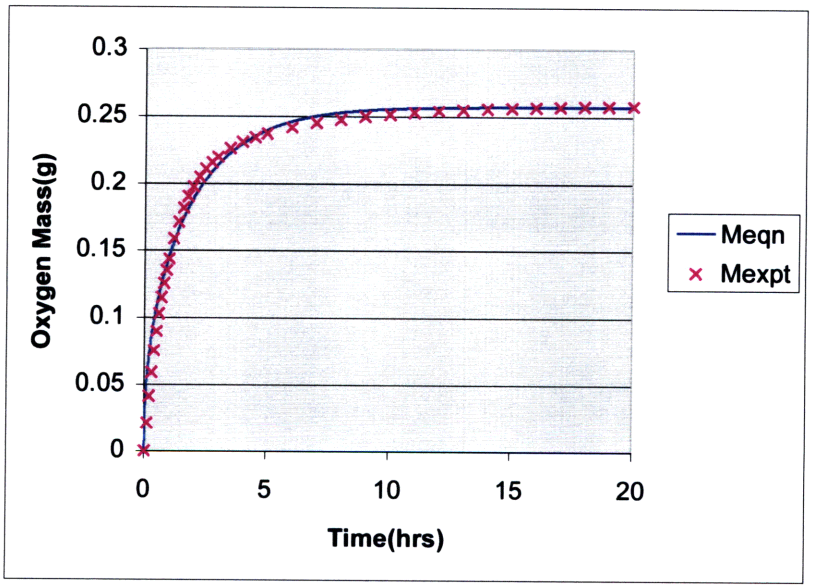

Figure 18: Oxygen Uptake of a Pellet at 800°C

Fitting curves for experiments at 600, 700, 800, and 900°C led to an equation that gave the effective diffusivity as a function of temperature. This D_{eff} is given by:

$$D_{eff} = 4.744 \times 10^{-9} \exp\left(\frac{-1670.54}{T}\right) \tag{46}$$

where T is in Kelvin and D_{eff} is in m^2/s.

Chapter 4 MODEL SOLUTION

4.1 Equations for Solid and Fluid Temperatures

4.1.1 One Dimensional Model

The 1D model consisted of fifty slices, each with a fluid and solid temperature. The subscript of the fluid temperature was i and the subscript of the solid temperature was 50+i. The value of i was indexed from 1 to 50 to cover every slice. Combining the heat flows and heat capacities within each slice of the 1D finite difference model gave an equation for the temperature of a fluid node described by the following:

$$\left.\begin{aligned} &Fluid_{HeatCap} = Conv_{in} + AirFlow_{in} - AirFlow_{out} - Rad_{out} \\ &C_1 \frac{dT_i}{dt} = C_2(T_{50+i} - T_i) + C_3(T_{i-1} - T_i) - C_4(T_i - T_{i+1}) - C_9(T_i - T_{\inf}) \\ &or \\ &C_1 \frac{dT_i}{dt} = -(C_2 + C_3 + C_4 + C_9)T_i + (C_2 T_{50+i} + C_3 T_{i-1} + C_4 T_{i+1} + C_9 T_{\inf}) \\ &K_1 \frac{dT_i}{dt} = -K_2 T_i + K_3 \end{aligned}\right\} \quad (47)$$

where C_1, C_2, C_3, C_4, and C_9 are given from Equations 8-16. For the solid node, the similar equation was given by:

$$\left.\begin{aligned} &Solid_{HeatCap} = Q_{gen} + Cond_{in} - Cond_{out} - Conv_{out} \\ &C_5 \frac{dT_{50+i}}{dt} = C_6 - C_2(T_{50+i} - T_i) + C_7(T_{49+i} - T_{50+i}) - C_8(T_{50+i} - T_{51+i}) \\ &or \\ &C_5 \frac{dT_{50+i}}{dt} = -(C_2 + C_7 + C_8)T_{50+i} + (C_6 + C_2 T_i + C_7 T_{49+i} + C_8 T_{51+i}) \\ &K_1 \frac{dT_{50+i}}{dt} = -K_2 T_{50+i} + K_3 \end{aligned}\right\} \quad (48)$$

where C_5, C_6, C_7, and C_8 are given by Equations 17-22.

4.1.2 Axisymmetric Model

In the axisymmetric model there were 200 different sections within the bed, 50 axial and 4 inner radial. The variable i was cycled from 1 to 50 as the axial component, and the variable n took on the values of 0 (for slices a), 50 (slices b), 100 (slices c), and 150 (slices d) to cover the radial sections. See Figure 8 and Figure 9 for a graphical explanation of the temperature indexes.

The inlet tube gas entered the top of the getter bed and was heated as it passed down through its inner tube. The temperature description of this heating can be found in Equation 23.

Moving outward radially through the bed, the next temperatures to be determined were the fluid and the solid temperatures. Combining the various heat flows and heat capacities for the sections in the axisymmetric model led to the following equation describing the fluid temperature:

$$\left.\begin{aligned} &Fluid_{HeatCap} = Conv_{in} + AirFlow_{in} - AirFlow_{out} - Conv_{wall} \\ &C_1 \frac{dT_{n+i}}{dt} = C_2(T_{200+n+1} - T_{n+i}) + C_3(T_{n+i-1} - T_{n+i}) - C_4(T_{n+1} - T_{n+i+1}) - C_{11}(T_{n+i} - T_{L,i}) \\ &or \\ &C_1 \frac{dT_{n+i}}{dt} = -(C_2 + C_3 + C_4 + C_{11})T_{n+1} + (C_2 T_{200+n+i} + C_3 T_{n+1-1} + C_4 T_{n+i+1} + C_{11} T_{w,1}) \\ &K_1 \frac{dT_{n+i}}{dt} = -K_2 T_{n+1} + K_3 \end{aligned}\right\} \quad (49)$$

The solid temperatures were again obtained by applying the first law of thermodynamics to the solid control volume defined by the squares in Figure 9 which led to the following:

$$\left.\begin{aligned} &Solid_{HeatCap} = Q_{gen} + Cond_{ax,in} - Cond_{ax,out} + Cond_{rad,in} - Cond_{rad,out} - Conv_{out} \\ &C_5 \frac{dT_{200+n+1}}{dt} = C_6 + C_7(T_{199+n+1} - T_{200+n+i}) - C_8(T_{200+n+i} - T_{201+n+i}) + \\ &.....C_{10,in}(T_{150+n+i} - T_{200+n+1}) - C_{10,out}(T_{200+n+1} - T_{250+n+i}) - C_2(T_{200+n+i} - T_{n+i}) \\ &or \\ &C_5 \frac{dT_{200+n+i}}{dt} = -(C_2 + C_7 + C_8 + C_{10,in} + C_{10,out})T_{200+n+i} + (C_6 + C_2 T_{n+i} + \\ &.....C_7 T_{199+n+1} + C_8 T_{201+n+i} + C_{10,in} T_{150+n+i} + C_{10,out} T_{250+n+i}) \\ &K_1 \frac{dT_{200+n+i}}{dt} = -K_2 T_{200+n+i} + K_3 \end{aligned}\right\} \quad (50)$$

where the radial conduction varied with n, or the given radial section.

The liner temperature, $T_{L,i}$, was found by equating the incoming heat to the outgoing heat. This led to the following equation:

$$\left.\begin{aligned} Liner_{HeatCap} &= Conv_{wall,in} - Rad_{out} \\ 3.3\frac{dT_{L,i}}{dt} &= C_{11}(T_{150+i} - T_{L,i}) - C_{12}(T_{L,i} - T_{w,i}) \\ 3.3\frac{dT_{L,i}}{dt} &= -(C_{11} + C_{12})T_{L,i} + (C_{12}T_{w,i} + C_{11}T_{150+i}) \\ K_1\frac{dT_{L,i}}{dt} &= -K_2T_{L,i} + K_3 \end{aligned}\right\} \quad (51)$$

The wall temperature, $T_{w,i}$, was found by equating the incoming radiation from the liner to the outgoing radiation to the intermediate shell, leading to the following equation:

$$\left.\begin{aligned} Wall_{HeatCap} &= Rad_{liner,in} - Rad_{coil,out} \\ 13.5\frac{dT_{w,i}}{dt} &= C_{12}(T_{L,i} - T_{w,i}) - C_9(T_{w,i} - T_{\inf}) \\ 13.5\frac{dT_{w,i}}{dt} &= -(C_9 + C_{12})T_{w,i} + (C_9T_{\inf} + C_{12}T_{L,i}) \\ K_1\frac{dT_{w,i}}{dt} &= -K_2T_{w,i} + K_3 \end{aligned}\right\} \quad (52)$$

4.1.3 Temperature Solution

The second to last equation in Equations 47-52 above was simplified to the following identical equation:

$$K_1\frac{dT}{dt} = -K_2T + K_3 \quad (53)$$

with constants K_1, K_2, and K_3 defined through Equations 47-52. Equation 53 then had the exact exponential solution of:

$$T_t = \frac{K_3 + (K_2T_{init} - K_3)\exp(\frac{-K_2t}{K_1})}{K_2} \quad (54)$$

where in the C program the initial temperature, T_{init}, was actually the temperature at the previous time step, $T_{t-\Delta t}$. The time step used in both models was 1 second, sufficiently small for an experiment that lasted over 3 hours. The choice of the time step did not require stability or convergence analysis because Equation 54 is an exact solution to Equation 53, though approximations to the bed were made in determining the constants K_1, K_2, and K_3.

4.2 C Program Steps for Solving Finite Difference Model

The initial temperature distribution within the bed was given by the steady state analysis of the bed with no internal reactions. Since almost every coefficient defined in Equations 8-29 above varied with temperature, it was necessary to evaluate the coefficients at each time step for the given slice temperature. Therefore, starting at the initial steady state temperatures, the program followed the general steps outlined below.

1) Began with initial time and initial temperatures
2) Found mass of oxygen absorbed by each section in time step (dt)
    - Kept track of previous mass in given section
    - Found rate of oxygen uptake for initial slices
    - Maximum oxygen absorbed (forcing term) was determined by the ratio of oxygen reaching that slice compared to initial inlet oxygen amount
    - Calculated pellet radius for given oxygen loading
    - Oxygen continued to reach higher slices until all oxygen was absorbed (looped through step (2) until all oxygen for given time step was absorbed or until end of bed was reached)
    - Oxygen breakthrough began once input oxygen rate exceeded uptake rate
3) Found inlet gas temperatures (bulk temperature)
4) Found liner and wall temperatures
5) Found fluid and solid temperatures
    - Calculated the 12 coefficients given section, temperature, oxygen mass, and previous oxygen mass
    - Calculated solid temperature
    - Calculated fluid temperature
    - Looped to step (5) until all temperature nodes were calculated
6) Incremented time and looped through (2) through (5) for all time

Appendix E gives the detailed code used to solve the axisymmetric model.

Chapter 5 RESULTS

The models predicted the transient temperature response of discrete points throughout the bed, given an unexpected intake of oxygen beginning at time zero. The initial bed was operating at steady state temperatures with no heat generation via oxidation when the input gas was suddenly switched from nitrogen to air.

5.1 One Dimensional Predictions

The one-dimensional program predicted that temperatures within the bed would rise to near 1225°C during air-ingress conditions. This maximum was less than that predicted by the axisymmetric model because the 1D model did not include a wall node temperature. This had the effect of radiating more heat away from the getter bed. The reaction took approximately 2.5 hours to complete with oxygen breakthrough predicted to begin around 1.2 hours. Figure 19 shows the temperatures within the bed, with a curve for each slice.

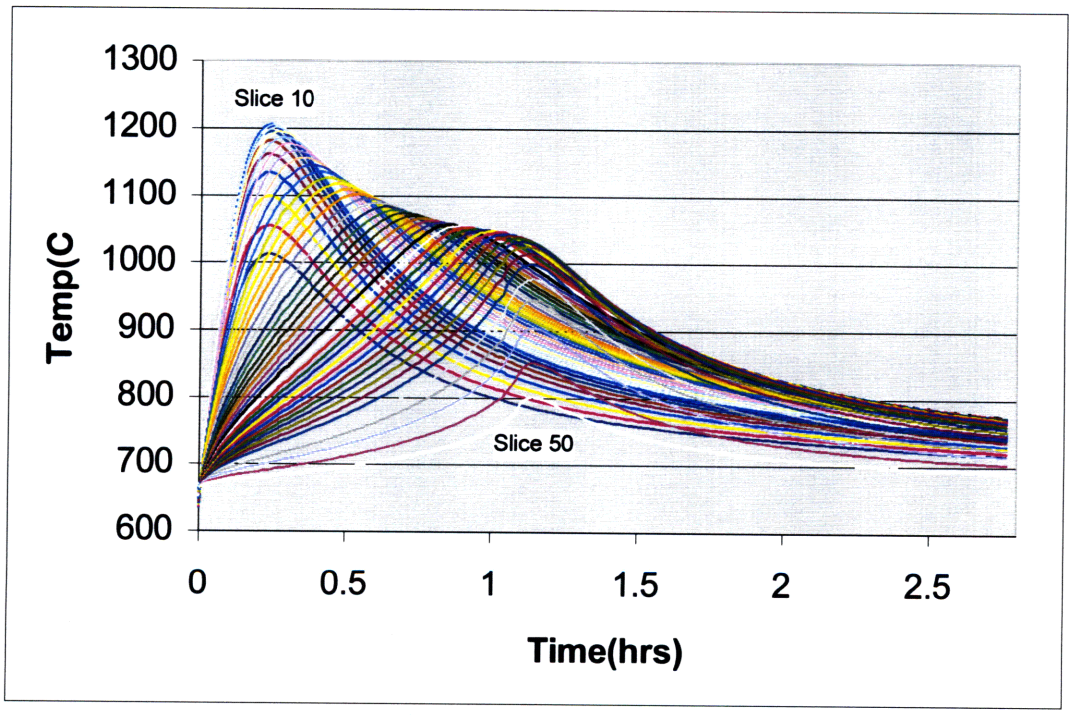

Figure 19: 1D Predicted Temperatures within bed

The rate of oxygen absorbed by the pellets varied with time and through the bed. The pellets in the last slice (50) began to oxidize slowly at first because the oxygen reaching them was scarce. As the beginning slices began to reach full loading, their uptake rate decreased and more oxygen made its way to the later slices. Though the reaction kept going until all the pellets were each fully loaded with 0.259 g O_2, once the uptake rate was exceeded by the input rate, breakthrough began. Hence, oxygen breakthrough was predicted to begin after 1.2 hours of the air-ingress experiment, but oxidation reaction continued at a rate lower than the input rate until the pellets were saturated.

5.2 Axisymmetric Predictions

The axisymmetric model was more accurate than the 1D model at predicting the getter bed temperatures during an air-ingress because it had more radial temperature nodes. Most importantly, it had separate temperature nodes for the inlet tube, liner and wall. Of the four radial sections within the bed, temperatures in the center section (A) are shown in Figure 20. Due to the conductivity of the bed, the inner temperatures were fairly similar. The maximum temperature reached within the bed was 1278°C, located 20% along the bed, and the reaction was mostly complete within two hours.

The inlet tube located along the center of the bed had an effect of slightly decreasing the temperature of the bed at the end sections. The gas flowed into the tube at the top of the bed near 400°C and reached 500°C after passing through the entire tube. Once exiting the tube, it turned around to flow up the bed, gaining more heat by first passing by the end cap and then flowing through the frit. At steady state, the inlet gas hitting the pellets was near 620°C.

Figure 20 shows that the inlet gas cooled the very first slices only slightly, hence the first slice reached a maximum of 1200°C. The hottest part of the bed was 14-30% down the length of the bed (Slices 7-15), reaching a maximum of 1278°C. Further down the bed than this, the slower reaction and cooling of the flowing gas meant that the maximum temperatures reached were a lower 1080°C. The end of the bed (Slice 50) reached its highest oxidation rate around one hour. Once the last slice began to oxidize as fast as it could, given that the oxide diffusing into the pellet material limited the reaction, the oxygen uptake of the bed as a whole was diminishing and breakthrough began.

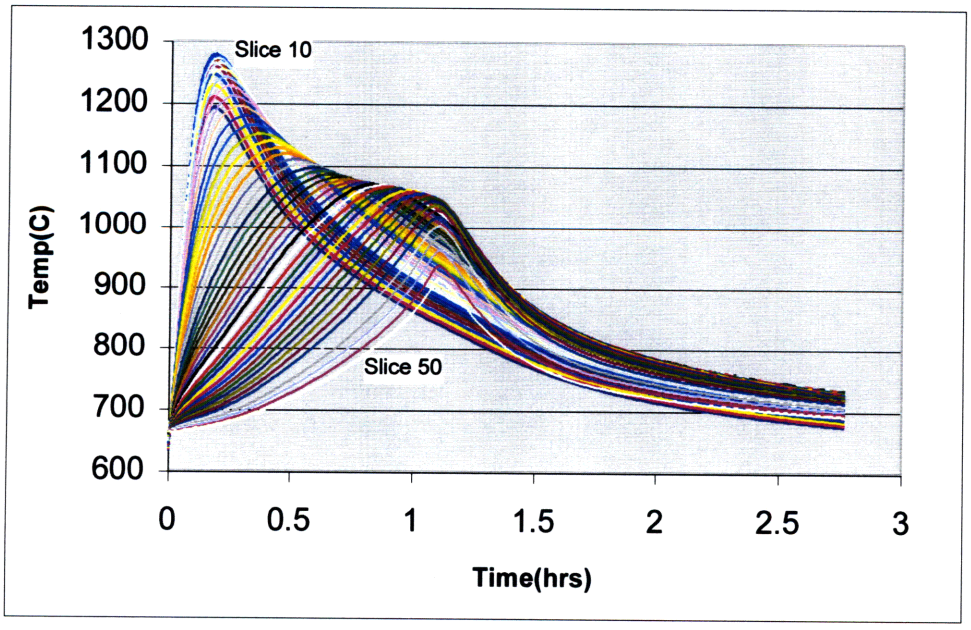

Figure 20: Predicted Bed Temperatures

The wall temperatures, shown in Figure 21, were seen to reach their maximum near slice 11, or 22% along the length of the bed. The peak temperatures predicted at the primary container were near 840°C, again cooling off within two hours.

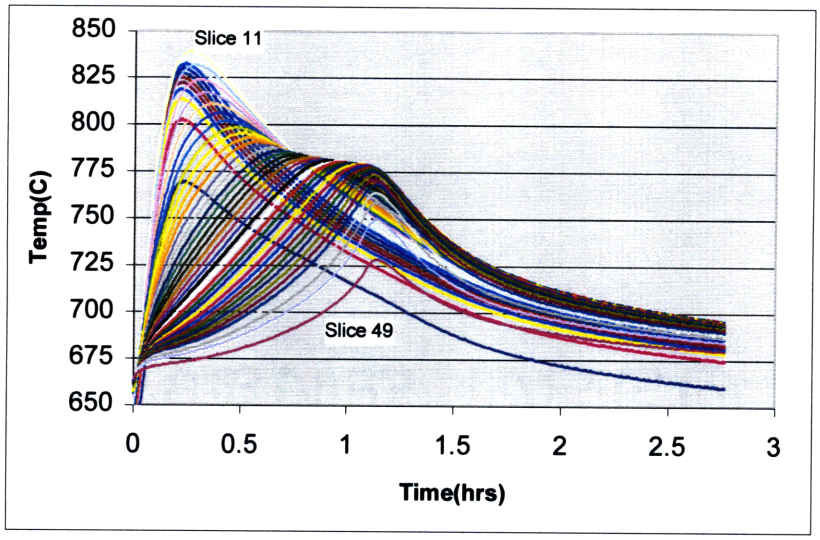

Figure 21: Predicted Wall Temperatures

The pellets were assumed to oxidize fully to 100% ideal loading, or 13.5 mol O_2/kg St-909. The individual pellets within slices 1-50 at the center of the bed absorbed oxygen as shown in Figure 22.

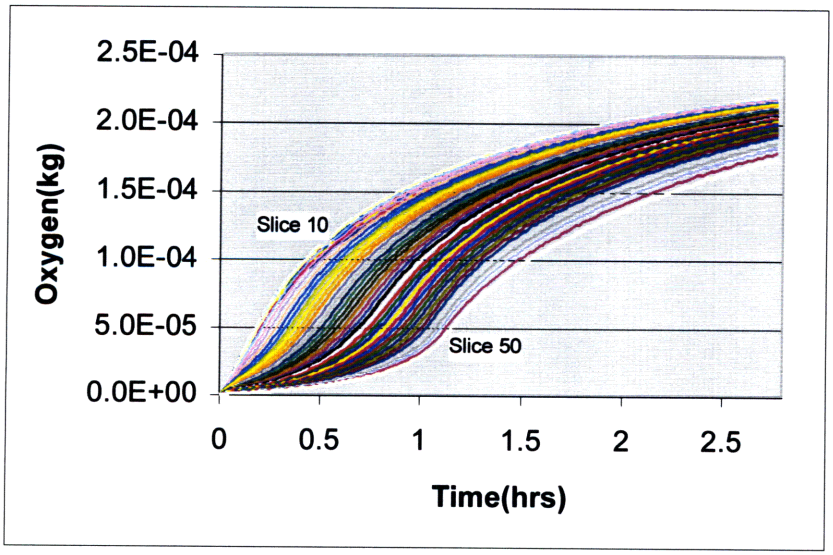

Figure 22: Predicted Oxygen Absorption

Slice 50 was predicted to absorb oxygen slowly for the majority of the first hour, while little oxygen was reaching it. Once the previous slices became saturated with oxygen, allowing the oxygen to proceed through the bed, Slice 50 started to react more vigorously. The oxygen breakthrough was predicted to begin at 55 minutes.

5.3 Experiment Results

The full-scale experiment had five internal thermocouples to measure the axial temperatures. The inner thermocouples were located at a radius of 1.6 cm (.625 in.). The thermocouples were located throughout the bed as follows: two at .965 cm (.38 in.), one at 2.24 cm (.88 in.), one at 7.32 cm (2.88 in.), and one at 12.4 cm (4.88 in.) from the end of the bottom frit. A schematic diagram of the thermocouple locations and their corresponding experimental temperatures are shown in Figure 23.

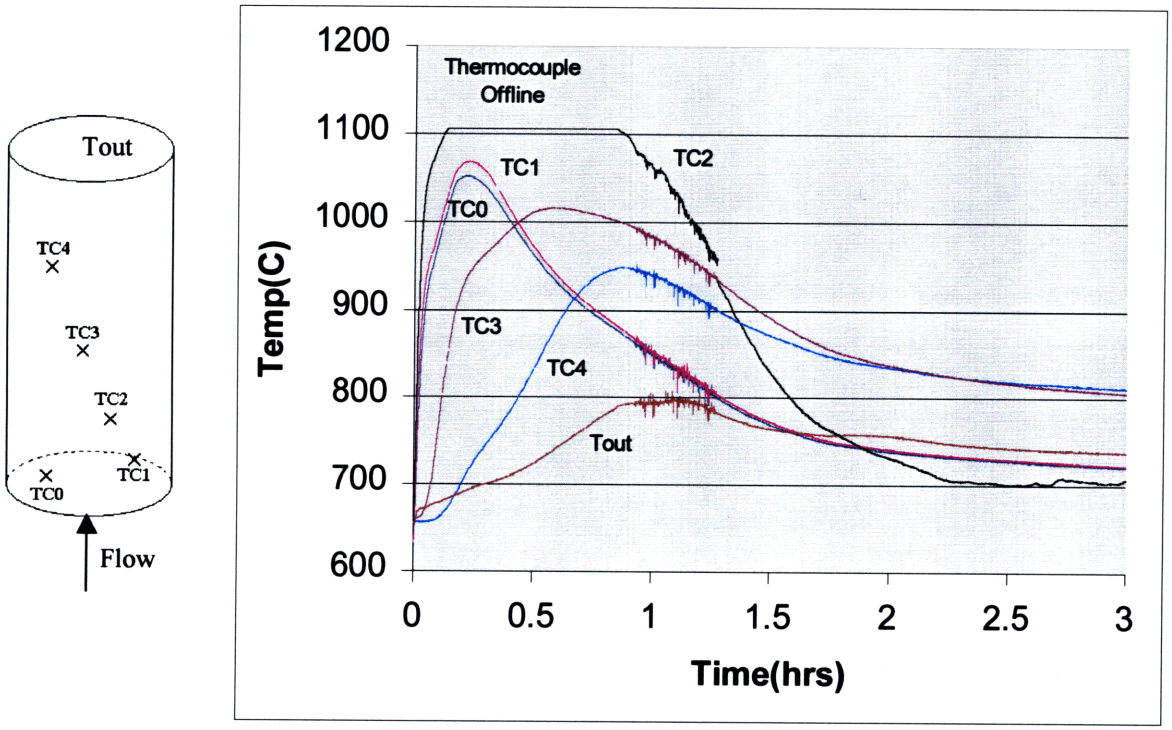

Figure 23: Experimental Internal Temperatures

The thermocouples were rated for temperatures up to 1372°C with an error of ±0.89%, or ±9.8°C at 1100°C (see Appendix A). As seen in Figure 23, the second thermocouple, TC2, went offline at 1100°C. This was due to an error in the data acquisition system (Labview), as the maximum voltage received from the thermocouple was exceeded. The fact that TC2 recovered after about one hour of the air-ingress experiment suggests that the real temperatures it was measuring did not exceed its rating of 1372°C. A curve fit to the experimental data for TC2 estimated that the temperature reached 1285°C.

There were seven external thermocouples tack welded onto the primary container of the getter bed. Their locations can be seen on the left of Figure 24. The measured external temperatures are not the absolute maximum temperatures that the primary container saw during the air-ingress experiment because the thermocouples were 50% along the length of the bed and the maximum temperatures seen were 20% along the length of the bed. The maximum external temperatures measured in the experiment were 810°C, a temperature which did not compromise the structural integrity of the primary container.

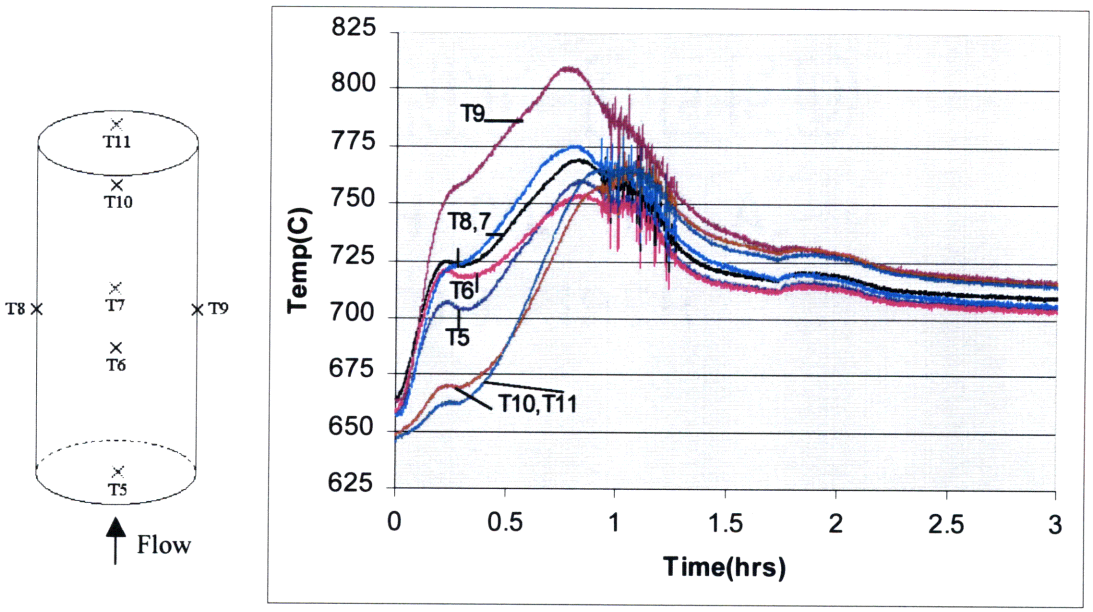

Figure 24: Experimental External Temperatures

The getter bed swelled about 2% radially at its centerline during the air-ingress experiment. This gradual swell can be seen at the midpoint of the bed in Figure 25.

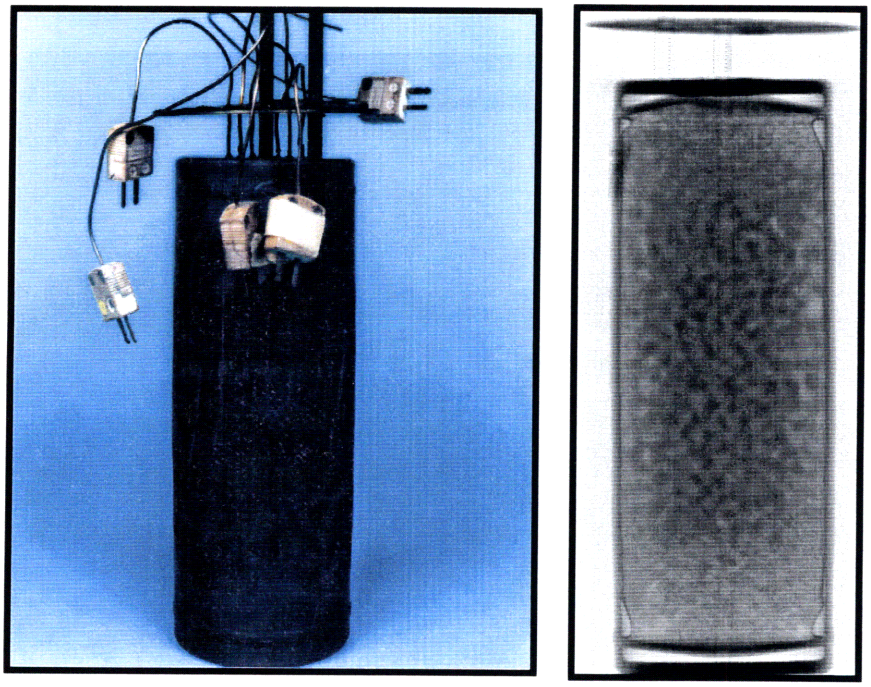

Figure 25: Getter Bed after Air-Ingress

Prior to the air-ingress experiment, the bed was preloaded with 2.5 mol N_2/kg St-909. Due to previous experiences where the St-909 pellets reacted with a small quantity of nitrogen and released heat in the reaction, the bed was preloaded with the nitrogen at a

low temperature. In normal operation, the system gas would consist mainly of nitrogen, such that the bed would be saturated with nitrogen during its initial start up stage. Steady state temperature measurements were also obtained from the bed with nitrogen flowing through the getter bed.

Though most of the reaction was completed within a few hours, the air-ingress experiment was allowed to run overnight. The swelling of the pellets had slowly continued as they kept absorbing a small amount of oxygen. After 8 hours of the experiment, all of the thermocouples went offline as they were ripped apart by the expanding pellets. The flow was held at 15 slm, but after 12 hours was restricted. The pellets had grabbed the inlet flow tube that was running down the center of the bed and pushed it into the bottom end cap, making the tube travel a total of .49 cm (.193 in.). This conclusion was based on an observed scoring of the end cap once the bed was disassembled and the position of the tube in the X-ray of the bed shown in Figure 25.

5.4 Comparison between Theory and Experiment

During the air-ingress experiment, the amount of oxygen that the pellets absorbed was close to their theoretical capacity. Since flow was kept near 15 slm, the oxygen input into the bed was 3 slm. Once the pellets' absorption rate dropped below the input oxygen rate, breakthrough began. This oxygen breakthrough was gradual and began after 50 minutes of the experiment, as shown in Figure 26. The axisymmetric model predicted that breakthrough would begin after about 55 minutes of the experiment. Figure 26 shows that the predicted and actual oxygen breakthrough characteristics were very similar.

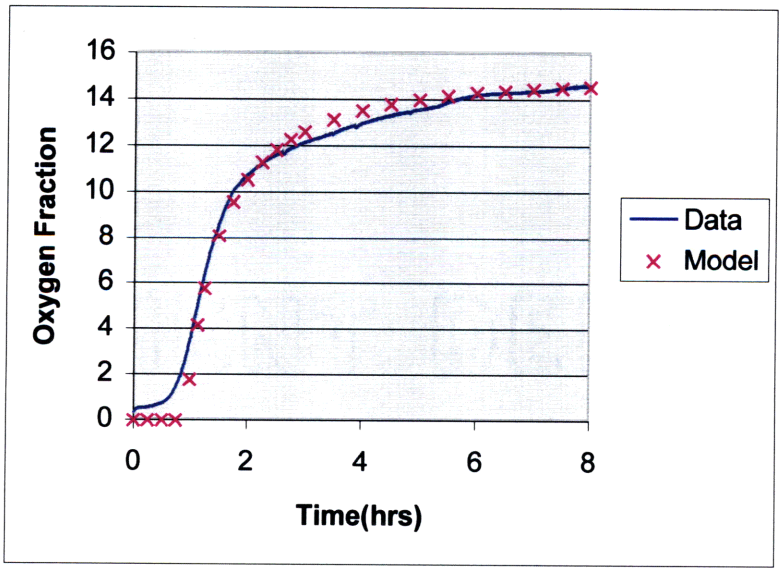

Figure 26: Oxygen Breakthrough Comparison

A comparison of the experimental temperatures to predicted temperatures shows a strong similarity, although the analysis predicts higher maximum temperatures than those

measured at locations further down the bed. A comparison between the thermocouple readouts and their corresponding slices can be found in Figure 27 through Figure 30.

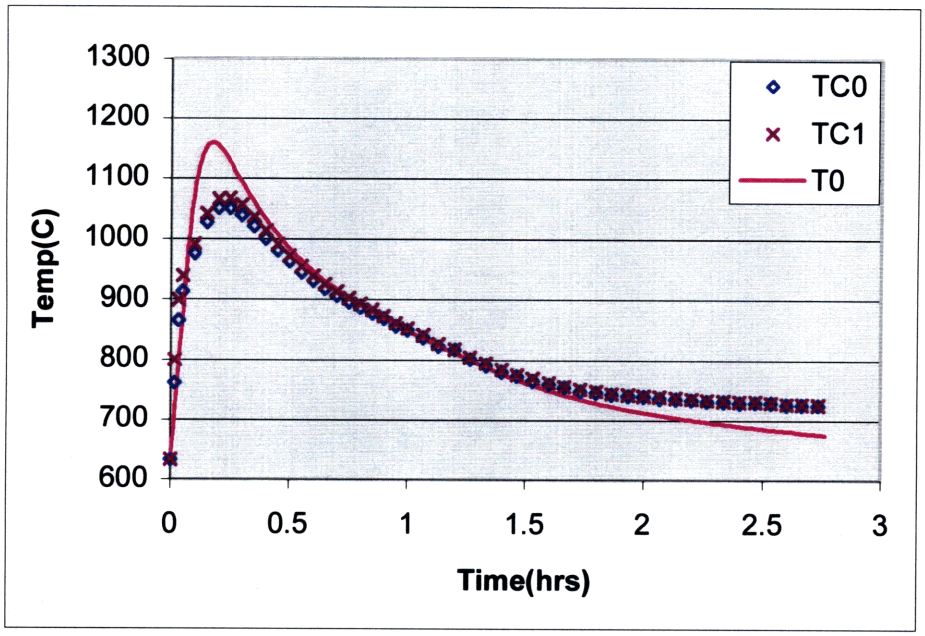

Figure 27: Axisymmetric TC 0 and TC1 Comparison

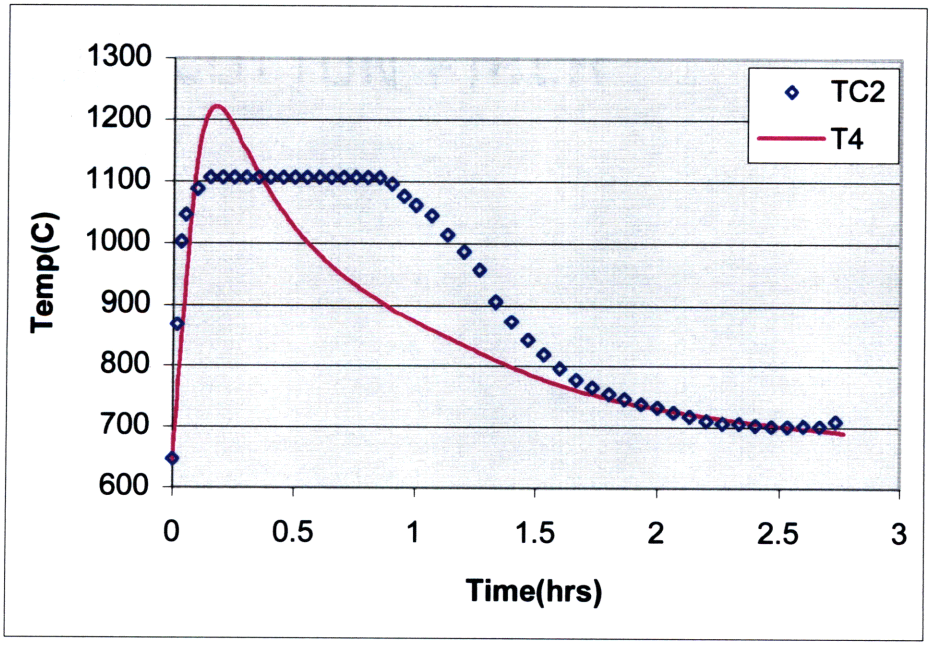

Figure 28: Axisymmetric TC 2 Comparison

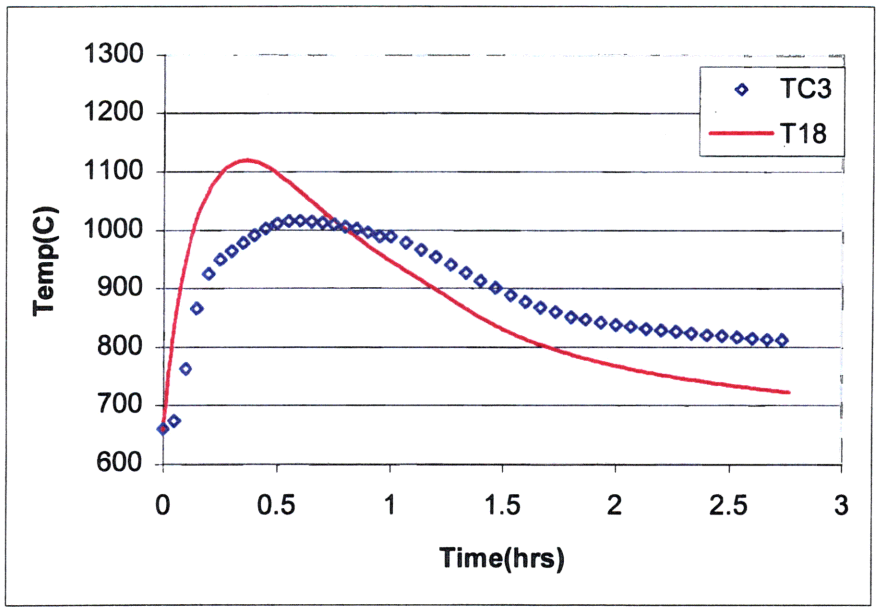

Figure 29: Axisymmetric TC 3 Comparison

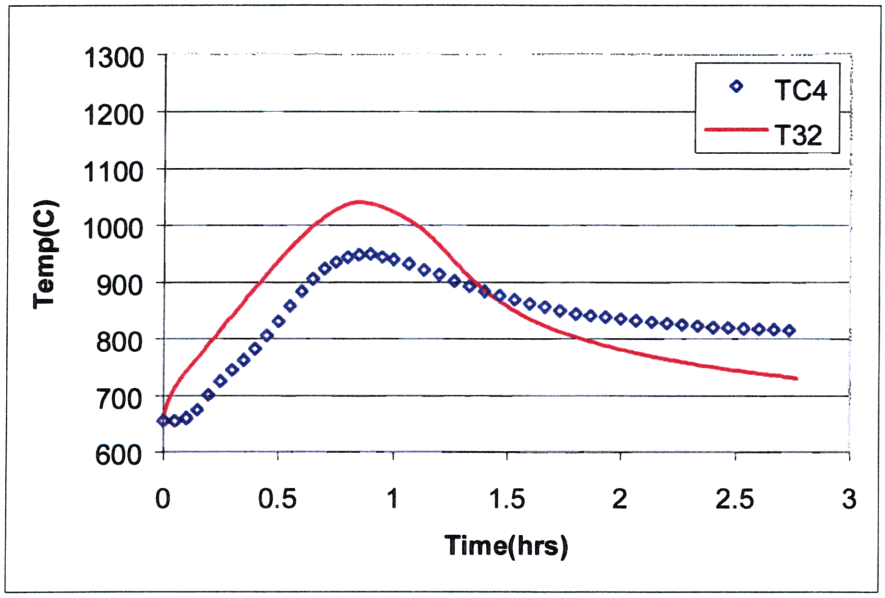

Figure 30: Axisymmetric TC 4 Comparison

Comparison between actual thermocouple measurements and predicted temperatures of the bed showed that the bed behavior agreed fairly closely. The maximum temperatures of the thermocouple 0 and 1 measurements were lower than those predicted (Slice 1), suggesting that the inlet gas was cooling the real pellets more than the predicted behavior. The rest of the agreement between thermocouples 0 and 1 and Slice 1 was strong, suggesting that the real initial bed oxygen absorption was very close to predictions.

These oxygen absorption predictions were dictated by the ODL model, which was based on single pellet experiments over temperatures ranging from 600 to 900°C.

The thermocouple 2 comparison showed strong initial similarity, though once the thermocouple went offline, it was had to determine the behavior of the real temperature. The real temperature appeared to behave as if its solid heat capacity was higher than that predicted.

The comparison between theory and experiment on thermocouples 3 and 4 showed similar behavior. The theory seemed to predict that the oxidation reaction would occur more quickly than in the actual system, as the temperatures reached were higher than the thermocouple readings and then cooled off more quickly. Since the oxidation behavior of the pellets with the ODL model was based on experiments up to 900°C, the diffusivity or reaction could've been limited at certain high temperatures, thereby reducing the reaction rate. In the TC 3 and TC 4 comparison, it also appeared that the heat capacity of the solid was higher in the experiment than that predicted.

A final comparison between prediction and experiment of the wall temperature can be seen in Figure 31.

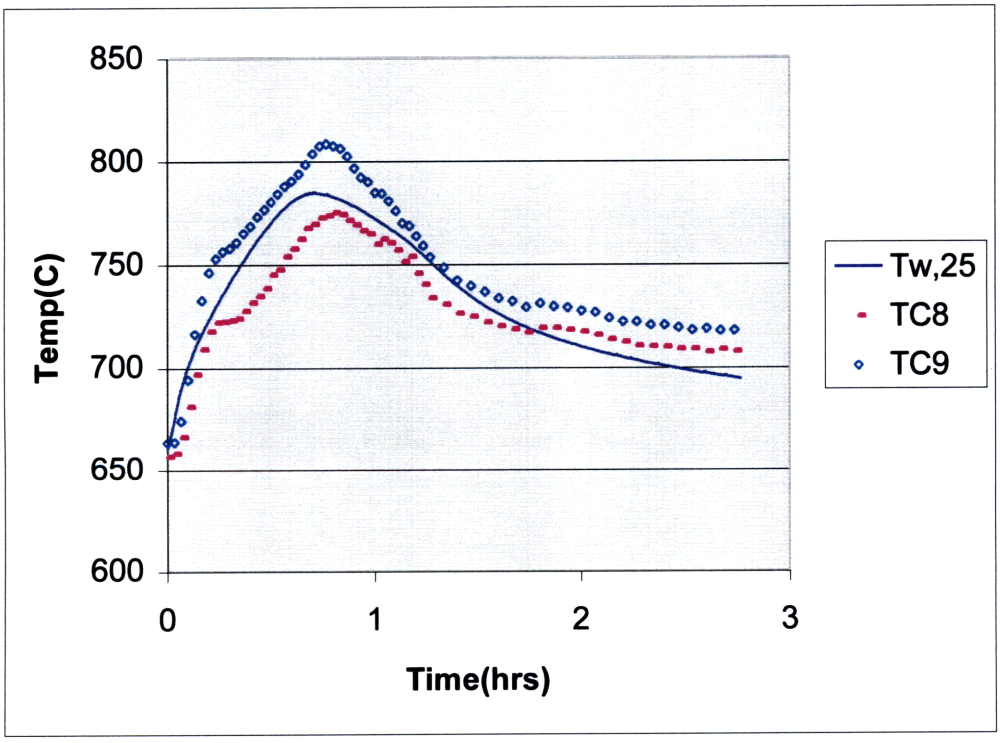

Figure 31: Axisymmetric Wall Temperature Comparison

The agreement between predicted wall temperatures and measured temperatures was seen to be very strong. The maximum wall temperatures predicted were 840°C located 20% along the bed length, about 50°C higher than the readings of TC 8 and TC 9, which were recorded at the midpoint of the bed.

Chapter 6 CONCLUSIONS

This thesis focused on a St-909 getter bed thermal failure analysis, which included laboratory tests and theoretical system models. Finite difference models using heat and mass transfer equations applied to the bed were developed for the LANL getter system. Small-scale experiments on individual St-909 getter pellets were performed and used to determine the oxygen absorption characteristics of the pellets. The oxidation was concluded to be limited by the oxide diffusing into the pellet material. The volume expansion characteristics with loading and the temperature dependence of this effective diffusivity were determined. A C-program was created and used to solve the finite difference equations, thereby determining the transient oxygen loading and thermal response of the getter bed.

Comparison of the models to experiments showed that the temperatures agreed fairly closely. In the full-scale air-ingress experiment, the pellets loaded to their maximum capacity and completed most of their reaction within two hours. The pellets themselves doubled in volume, first filling up the void space within the bed and then expanding into the crush zone. The primary container swelled almost 2% radially during the experiment, an improvement over previous experiments with getter beds performed at LANL where the swelling had been 8-10% at full loading. Oxygen breaking through the bed, which would then flow through the tritium absorption bed in a full glovebox loop setup, was gradual and began after one hour of air-ingress conditions.

Future designs of getter beds will be adjusted only slightly from the experimental case, as this system design used at LANL was seen to successfully withstand the extreme temperature conditions of an air-ingress. The steel wool packed at the bottom of the getter bed will be changed to a more coarse steel wool so that it would maintain its shape more easily and not burn up, therefore protecting the frits from deformation. The addition of the liner to create a crush zone was a successful addition in this experiment and swelling of the bed was reduced from previous getter bed experiments. The gas inlet tube should be notched with an uneven end so that flow will not be completely restricted should the pellets swell enough to push the tube into the end cap. Positioning the inlet gas flow down the center of the bed had two positive effects: the first being that during normal operation the gas was heated from its preheater exit temperature closer to its operation temperature, and the second being a slight cooling of the getter bed at its potentially hottest section.

Should a possible equipment failure or accident occur causing a break in a line of a glovebox gas cleanup loop, the resulting air-ingress into a St-909 getter bed will not cause the bed to fail by overheating. The maximum temperatures reached within the bed will approach 1280°C, but the primary stainless steel container will stay below 840°C, and as this experiment illustrates, it will maintain its structural integrity.

NOMENCLATURE

a	surface area of pellets per bed volume [1/m];
A_c	cross-sectional area of bed [m^2];
A_p	pellet surface area [m^2];
A_{surf}	outer surface area of bed [m^2];
c_p	specific heat [J/kgK];
$\widetilde{C}$	heat generation coefficient [J/kg St909];
d	diameter [m];
D	diffusivity of oxide into pellet [m^2/s];
ΔG°	Gibbs energy of formation of an oxide [J/mol];
G	fluid mass velocity per unit area of bed cross-section [kg/sm^2];
ΔH°	Enthalpy of formation of an oxide [J/mol];
h_p	heat transfer coefficient, pellet to fluid [W/m^2K];
h_w	heat transfer coefficient at wall [W/m^2K];
k	thermal conductivity [W/mK];
Δl	thickness of finite difference slice, bed length/50 [m];
L	characteristic length of bed [m];
$\dot{m}$	mass flow rate [kg/s];
M	mass of oxygen within pellet [kg];
n	number of pellets;
P	heat transfer perimeter [m];
Pr	Prandtl number;
Q	volume flow rate [m^3/s];
Re	Reynolds number associated with packed bed flow, $V\rho x/\mu$;
R_p	radius of a pellet [m];
R_T	column radius [m];
Δt	time step [s];
T	temperature [K];
V	velocity [m/s];
V_p	volume of pellet [m^3];

Greek symbols

ε_b	void fraction within bed [initially 0.48];
ε	emissivity;
μ	viscosity [kg/ms];
ρ	density [kg/m^3];
σ	Stephan-Boltzman's constant [5.67E-8 W/m^2K^4];

Subscripts

0	inlet;
ax	axial;
b	bulk, fluid in tube;
eff	effective;
f	fluid/air;
i	slice number;
inf	infinite;
init	initial;
L	liner;
O_2	oxygen;
p	pellet;
r	radial;
s	solid/getter material;
surf	surface;
t	at time t;
w	wall;

LIST OF WORKS CITED

Achenbach, E., "Heat and Flow Characteristics of Packed Beds", *Experimental Thermal and Fluid Science*, Elsevier Science Inc., New York (1995).

Baker, J. D. and Tuggle, D. G., "Tritium purification via zirconium-manganese-iron alloy getter St-909 in flow processes" (1993).

Gyftopoulos, Elias P., and Beretta, Gian Paolo, *Thermodynamics Foundations and Applications*, Macmillan Publishing Company, New York (1991).

Incropera, Frank P. and De Witt, David P., *Fundamentals of Heat and Mass Transfer*, Wiley & Sons, New York (1990).

Lide, David R. Editor-in-Chief, *CRC Handbook of Chemistry and Physics*, CRC Press (1994).

Mills, Anthony F., *Basic Heat and Mass Transfer*, Irwin, Concord, MA (1995).

Poulikakos, D., *Conduction Heat Transfer*, Prentice-Hall, Englewood Cliffs, NJ (1994).

Wakao, N. and Kaguei, S., *Heat and Mass Transfer in Packed Beds*, Gordon and Breach Science Publishers, New York (1982).

Welty, Wicks, & Wilson, *Fundamentals of Momentum, Heat, and Mass Transfer*, Wiley & Sons, New York (1976).

Appendix A: Summary of Experimental Results

Pressure Behavior

The pressure plots obtained from small-scale experiments had two sections to their curves. During the beginning of the experiment, the pressure would drop sharply indicating a high oxygen uptake rate, and as time progressed, the uptake rate would slow substantially. This behavior was represented by a sum of two exponential expressions, each with their own magnitude and time constant. Starting near 570 torr, the pressure would drop close to the offset pressures shown in Table A1. Equation A1 shows how the experimental pressure relates to the given quantities in Table A1.

$$P = offset + \Delta P_1 \exp(-t / tau_1) + \Delta P_2 \exp(-t / tau_2) \qquad \text{(A1)}$$

where ΔP_1 and $1/tau_1$ are from the first line given for a set of data in Table A1. Table A1 also gives the experimental temperature, the number of pellets used, the achieved loading, and whether or not the reaction was complete.

Table A1: Experimental Curve Fits

Temp (C)	#pellets	Loading mol O_2/kg909	complete?	ΔP (torr)	ΔP %	1/tau (1/hrs)	offset (torr)
600	1	8.8	Yes	24.31	33.1	1.203	491.84
				49.13	66.9	0.217	
600	1	5	No	7.75	18.4	2.887	523.93
			no time	34.39	81.6	0.556	
600	2	7.81	No	39.74	34.6	1.26	450.3
			no O2	74.98	65.4	0.569	
600	3	5.04	No	12.3	10.2	22.21	444.8
			no O2	107.82	89.8	0.967	
650	6	3.45	No	56.2	34.6	9.37	369.7
			no O2	106.3	65.4	0.73	
650	6	2.86	No	47.16	30.1	5.993	427.95
			no O2	109.42	69.9	0.471	
700	1	13	Yes	61.34	64.7	0.799	475.12
				33.49	35.3	0.0886	
800	1	13.5	Yes	74.68	77.2	1.089	473.18
				22.01	22.8	0.208	
900	1	11.46	Yes	44.07	56.9	1.734	487.94
				33.34	43.1	0.109	

The flow rate within the system was near 700 cubic centimeters per minute. An example pressure plot can be found in Figure A1. The curve fit described by the parameters in Equation A1 and given in Table A1 is seen to match the experimental pressure exactly. The curve fits for the various experiments are used for behavioral comparisons as well as comparisons to the ODL model in order to determine the effective oxide diffusivity into the ZrMnFe pellet.

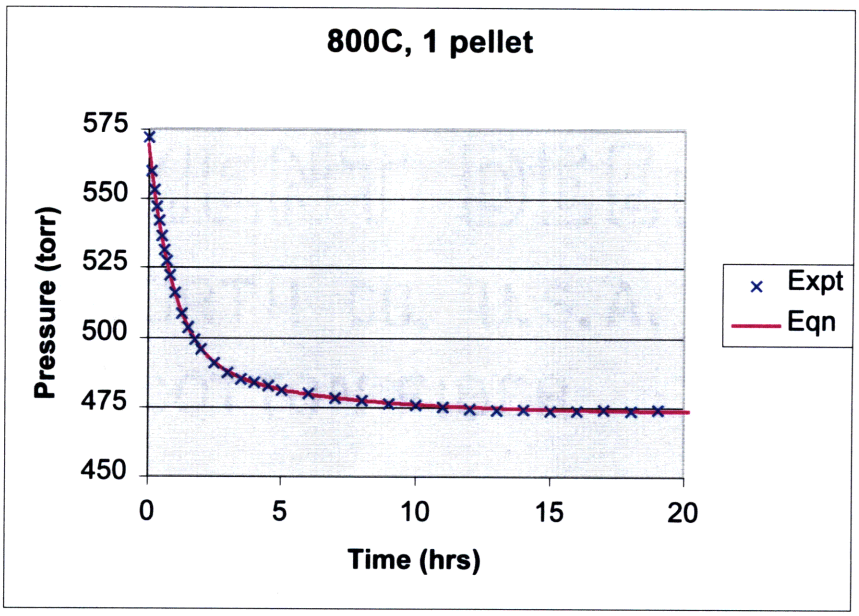

Figure A1: Pressure Decrease from 1 Pellet at 800°C

Mass Loading

The loading in the experiments was determined by weighing the pellet both before and after the oxidization and assuming all of the added mass was oxygen. This assumption is confirmed by the mass spectrometer output data shown in Figure A2. The St-909 pellets do absorb some nitrogen, but they saturate quickly and getter oxygen preferentially over the nitrogen.

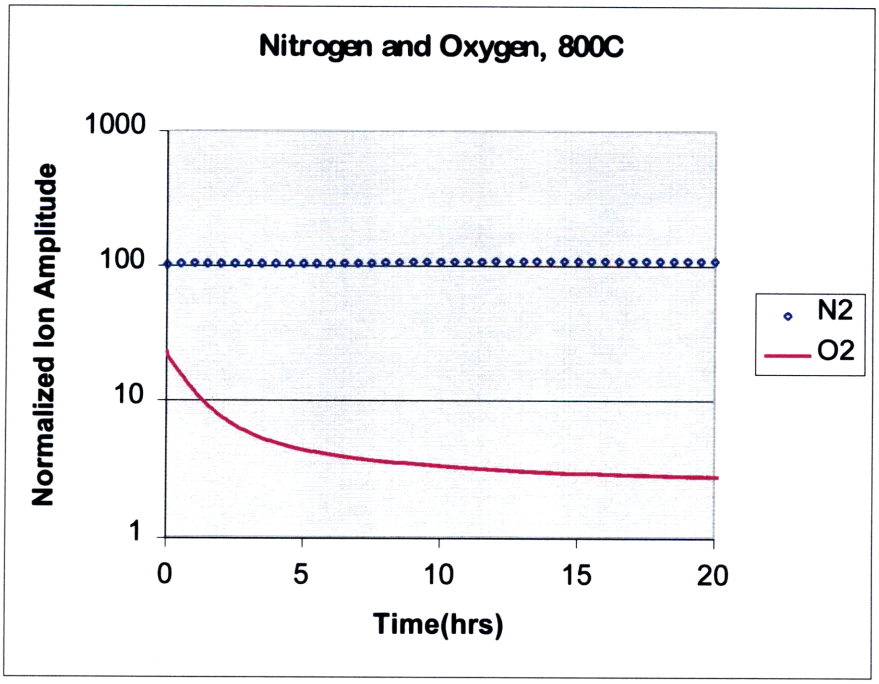

Figure A2: Mass Spectrometer Normalized Output, 800°C

The equation for the experimental mass uptake was then taken from the pressure curve fits to yield Equation A2.

$$M = M_{tot}[\Delta P\%_1(1-\exp(-t/tau_1)+\Delta P\%_2(1-\exp(-t/tau_2)] \quad \text{(A2)}$$

This equation for the mass of oxygen within the pellet was then compared to the ODL model to find the effective diffusion coefficient of metal oxide into the St-909 pellet.

Uncertainty Analysis

The thermocouples used were Type K and had an accuracy to within ±2.2°C or ±0.75%, whichever was greater. Therefore, a measurement of 1100°C was accurate to within 8.25°C.

The data acquisition system, Labview DAQ/SCX1 was accurate to within ±0.02% on the voltage input readings. Conversion from voltage to temperature was given by the following equation:

$$\begin{aligned} T &= 4.9252x10^{-8}V^6 - 8.742x10^{-6}V^5 + 5.9534x10^{-4}V^4 \\ &-1.7652x10^{-12}V^3 + 1.9384x10^{-1}V^2 + 2.391x10^{1}V \end{aligned} \quad \text{(A3)}$$

Taking the most significant voltage variation (T=23.91*V), the error for the temperature reading was then ±0.4782%, calculated from the following equation:

$$\varepsilon_T = \sqrt{(23.91\varepsilon_V)^2} \quad \text{(A4)}$$

Summing the two errors lead to a worst case error (WCE) of ±1.2282%, or ±13.51°C with a true 1100°C reading. The total probable error (TBE) was obtained using the root sum square (RSS) method and gave an error of ±0.89%, or ±9.784°C for a reading of 1100°C.

The oxygen sensor used was a Nyad, Inc. sensor. There was no manual available to give its accuracy. Model 232's two-channel oxygen readout was used with a model OS1 sensor.

Additional Experimental Results

The data above, given in Table A1, was obtained from the loop experimental setup. Prior to using the loop setup, several tests were performed with a stagnant volume of air reacting with a single pellet. This stagnant setup can be seen in Figure A3, where all of the lines represent ¼ in. tubes. As in the loop setup, the total pressure within the volume was measured as a function of time to determine the mass uptake of a single St-909 pellet. The pellets initially absorb oxygen quickly and then more slowly such that the

resulting mass uptake looks exponential in form. Ideally, a single 0.6 g St-909 pellet will absorb up to 13.5 mol O_2/kg St-909 pellet material. The pellet also has the capacity to absorb a certain amount of nitrogen before saturation, which amounts to near 2 mol N_2/kg St-909.

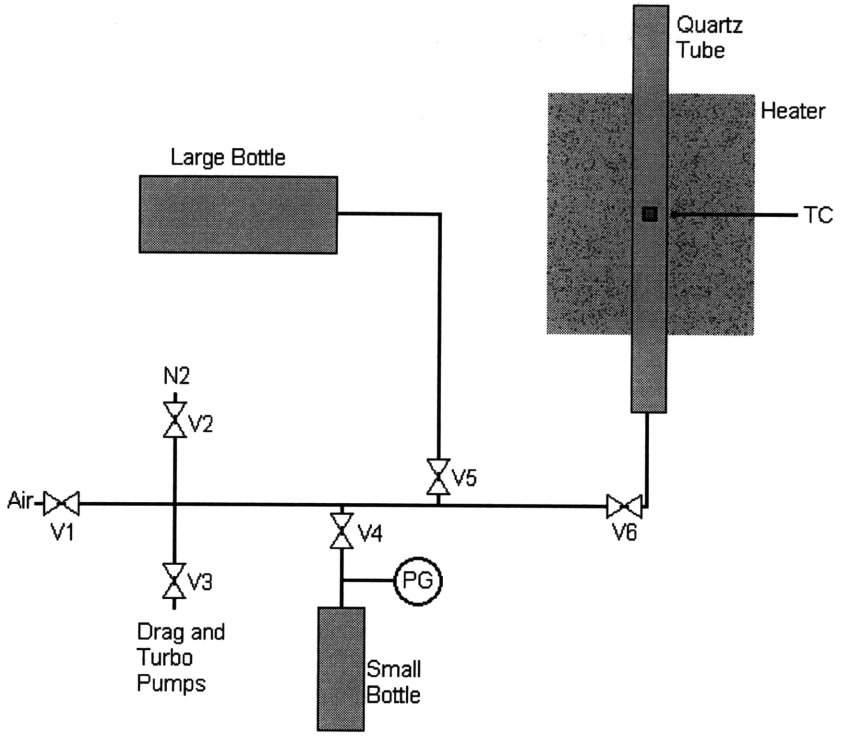

Figure A3: Stagnant Experimental Setup

For these stagnant experiments, the following steps were followed.

10. Fittings greased around quartz tube with high vacuum grease.
11. Volume pumped down to below 5 millitorr.
12. Temperature raised on quartz tube with heater to set point (e.g. 600 °C). Held under vacuum at high temperature for two hours to activate 909 pellet.
13. Quartz volume isolated under vacuum (valve 6).
14. Pump cut off (valve 3).
15. Entire rest of volume (1316 cc) filled with air (valve 1).
16. Labview started to record pressure and temperature of system.
17. Valve 6 opened (volume to 1527 cc). Labview captured pressure versus time response for system.
18. After reaching a pressure steady state, heater turned off and cooled.

The loadings achieved under these stagnant load conditions were much lower than expected at only 15% of ideal loading. The mass convection term was very low, causing average lodings near 2 mol O_2/kg St-909, as is shown in Table A2. In experiments #1-4, air was used within the system. In experiment #5, pure nitrogen was first introduced into

the system for several hours, and then the system was filled with air. This was to determine the effect of nitrogen on the pellets.

Table A2: Stagnant Experimental Results

No.	Experiment	mO_2 (g)	mol /kg 909	Pressure Drop (torr)
1	600C#1, Air	0.04	2.12	529-516=13
2	600C#2, Air	0.04	2.05	528-515=13
3	650C, Air	0.05	2.65	530-515=15
4	700C, Air	0.05	2.6	527.5-510=17.5
5	600C, N_2	[0.0362]	[2.15]	Initial 866, [16.25]
	then Air	0.0338	1.76	528-517=11

The loading factor for these experiments was determined by initial and final weights of the pellet. The loading was then calculated using the following formula, which assumed that all of the added mass was oxygen.

$$\text{load [mol } O_2\text{/kg 909]} = [m_f(g) - m_i(g)] * (1 \text{ mol } O_2/32 \text{ g})/m_i(kg) \qquad \text{(A3)}$$

An example pressure plot from these stagnant experiments can be seen in Figure A4.

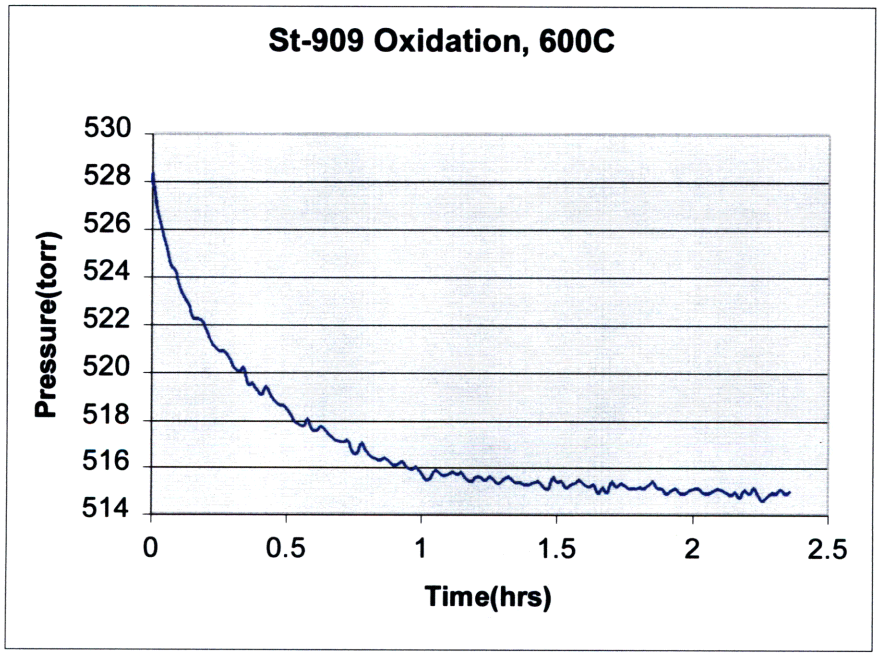

Figure A4: Stagnant Experimental Pressure

From the loadings given in Table A2, it is seen that at the higher temperature of 650°C, the pellet did absorb more oxygen from the air. The pressure dropped 14.3 torr at 650°C, compared to 12.6 torr at 600°C.

Nitrogen within the system in experiment #5 was at a pressure of 866 torr initially, or 1.5 times atmospheric pressure. The nitrogen was absorbed quickly at first, and the pressure

continued to decline for almost 23 hours to 765 torr. The air experiment then acted in a similar manner as previous experiments, with a slight decrease in oxygen absorption.

The stagnant pressure drop for experiment #5 was 11.54 torr, compared to 12.56 torr for experiments #1-2. The overall effect that the nitrogen had on the pellet oxygen absorption characteristics was only a slight decrease in the loading capacity.

Appendix B: Thermal Properties of Air versus Temperature

For several of the coefficients needed to compute the fluid and solid temperatures, the fluid property variance with temperature is required. The following data for density, specific heat, viscosity, and thermal conductivity was obtained from Mills (1995).

Density

Density varies exponentially with temperature, as is show in Equation B1 and Figure B1.

$$\rho_f = .142178 + 1.103286 \exp(-.00165T) \tag{B1}$$

where ρ_f is in kg/m^3 and T is in Kelvin. This is a curve fit that minimizes the standard deviation for the temperature range that the getter bed operates over, i.e. 900-1500K. The standard deviation of the density described by the equation and that tabulated in Mills was 1.04x10^{-4} kg/m^3 (~0.03%).

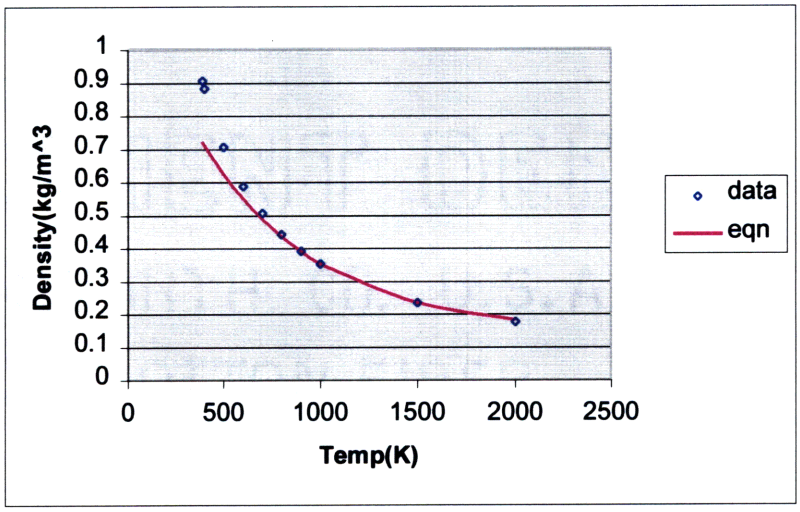

Figure B1: Air Density Variation with Temperature

Specific Heat

The specific heat of air varies exponentially with temperature, as is shown in Equation B2 and Figure B2.

$$c_{p,f} = 891.3907 + 495.6262[1 - \exp(-.00636T)] \tag{B2}$$

where $c_{p,f}$ is in J/kgK and temperature T is in Kelvin. Again, the curve fit is for the desired temperature range where the standard deviation of specific heat between equation and data was 5 J/kgK (~0.45%).

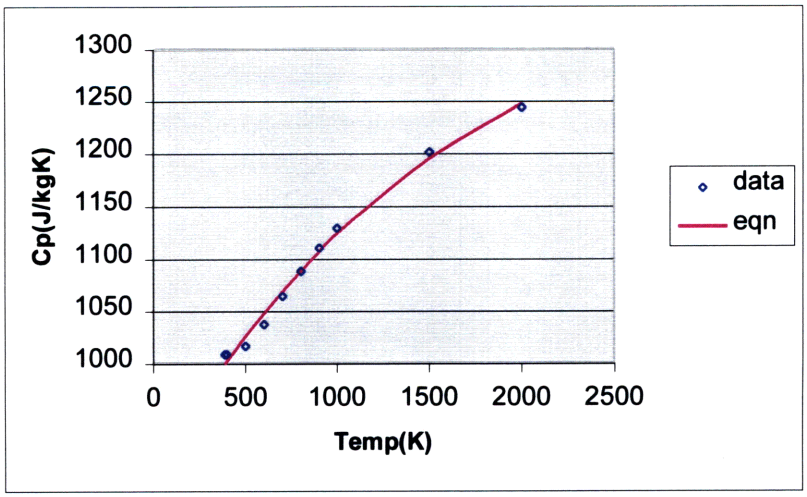

Figure B2: Air Specific Heat Variation with Temperature

Viscosity

Viscosity varies linearly with temperature, as is shown in Equation B3 and Figure B3.

$$\mu_f = (16 + .0252833T) \times 10^{-6} \tag{B3}$$

where μ_f is in kg/ms and T is in Kelvin. The standard deviation of viscosity between equation and data was 0.28 kg/ms (~0.56%).

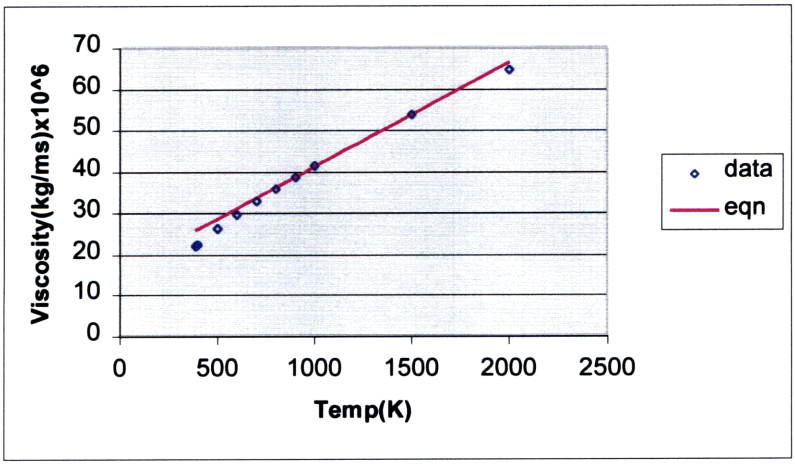

Figure B3: Air Viscosity Variation with Temperature

Thermal Conductivity

Thermal conductivity also varies linearly with temperature over the desired temperature range, as shown in Equation B4 and Figure B4.

$$k_f = .015 + 5.1666 \times 10^{-5} T \tag{B4}$$

where k_f is in W/mK and T is in Kelvin. The standard deviation of the thermal conductivity between equation and data was 5.5×10^{-4} W/mK (~0.69%).

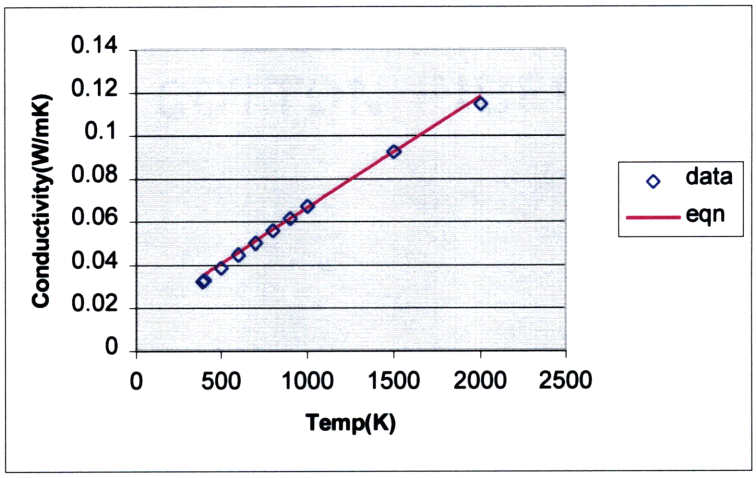

Figure B4: Air Thermal Conductivity Variation with Temperature

Appendix C: St-909 Pellet Characteristics

Heat Generation

If all of the Zr, Fe, and Mn within a pellet are oxidized, the pellet will release 3.9 kJ of heat. This heat generated within a pellet depends on the enthalpy of formation, which is related to the Gibbs energy of formation associated with the particular exothermic oxidation reaction. St-909 pellets are 40.5% Zr, 25% Fe, 24.5% Mn, and 10% Al. The aluminum, however, does not tend to oxidize and acts mostly as a binder. Also, at operating temperatures the aluminum is at and above its melting temperature of 660°C, another reason to believe that it does not oxidize.

The Gibbs energy of formation of a metal oxide is found by using Equation C1 (Lide, 1994).

$$\Delta G^\circ = A + BT + CT\log_{10} T \tag{C1}$$

where ΔG° is in J/mol and T is in Kelvin. The constants A, B, and C vary with the oxidizing metal and are given in Table C1 for the metals in St-909 pellets (Lide, 1994).

Table C1: Constants for Oxidation of Zr, Fe, and Mn

Reaction	Temp Range(K)	A	B	C
$Zr+O_2 \rightarrow ZrO_2$	300-1800	-1100032	245.21	-7.56
$Fe+.5O_2 \rightarrow FeO$	300-1800	-270590	72.64	-1.26
$Mn+.5O_2 \rightarrow MnO$	300-1500	-383209	56.68	2.15

To find the heat released from the pellet reaction, using the Gibbs energy relations, Equation C2 is used (Gyftopoulos, 1991). Equation C3 results from combining C1 and C2.

$$\left.\frac{\partial\left(\Delta G^\circ/T\right)}{\partial T}\right|_p = \frac{-\Delta H^\circ}{T^2} \tag{C2}$$

$$\Delta H^\circ = A - CT/\ln(10) \tag{C3}$$

The entropy term involved in the oxidation reaction is negative because the gaseous oxygen atoms are forming a more ordered solid oxide, the enthalpy of formation ends up being 10-15% more negative than the Gibbs energy of formation.

Since a single pellet has the mass of near 0.6 g, the moles of zirconium, iron, and manganese within one pellet are all close to 0.00267 mol/pellet (see Table C2 below). Maximum loading at 13.5 mol O_2/kg 909 for a 0.6 g pellet would getter 0.2592E-3 kg O_2/pellet. The heat generated per pellet then depends on:

$$\left.\begin{aligned}\widetilde{C} &= .00267\frac{mol}{pellet}\frac{pellet}{.2592\times10^{-3}\,kgO_2}(\Delta H^{\circ}_{Zr}+\Delta H^{\circ}_{Fe}+\Delta H^{\circ}_{Mn})\frac{J}{mol}\\ \widetilde{C} &= 10.3(\Delta H^{\circ}_{Zr}+\Delta H^{\circ}_{Fe}+\Delta H^{\circ}_{Mn})\frac{J}{kgO_2}\end{aligned}\right\} \quad \text{(C4)}$$

This $\widetilde{C}$ gives the energy released by a single pellet per amount of oxygen oxidized.

Property Data

Some basic characteristics of the individual metals within the pellets can be found in Table C2 (Mills, 1995 and Incropera, 1990).

Table C2: Property Characteristics of Zr, Fe, Mn, and Al

Metal	Molar Mass	Density	Conductivity	Specific Heat, J/kg K					
	g/mol	kg/m^3	W/mK	300K	800K	1000K	1200K	1500K	2000K
Zr	91.224	6570	22	278	342	362	344	344	344
Fe	55.847	7874	35	449	680	975	609	654	
Mn	54.938	7440	7.82	480					
Al	26.982	2700	220	900	1180	1225	aluminum oxide		

The specific heat varied with temperature. This variation was modeled using the following equation:

$$c_p = \frac{Amp}{\sigma^2}(T - T_{offset})\exp\left(\frac{-(T-T_{offset})^2}{2\sigma^2}\right) + c_{p,offset} \quad \text{(C5)}$$

where the parameters Amp, σ^2, T_{offset}, and $c_{p,offset}$ can be found in Table C3. These parameters were determined by curve fitting Equation C5 to the available data over the temperature range of 800 to 1600 K. Manganese was assumed to have similar characteristics as iron. Aluminum was assumed to have a constant specific heat of 1200 J/kgK.

Table C3: Specific Heat Temperature Variation Parameters

Metal	Amp	σ^2	T_{offset}	$c_{p,offset}$
Zr	4500	22,000	810	344
Fe	80,000	22,000	810	647.7

The curve fits for the specific heats of zirconium and iron can be seen in Figure C1.

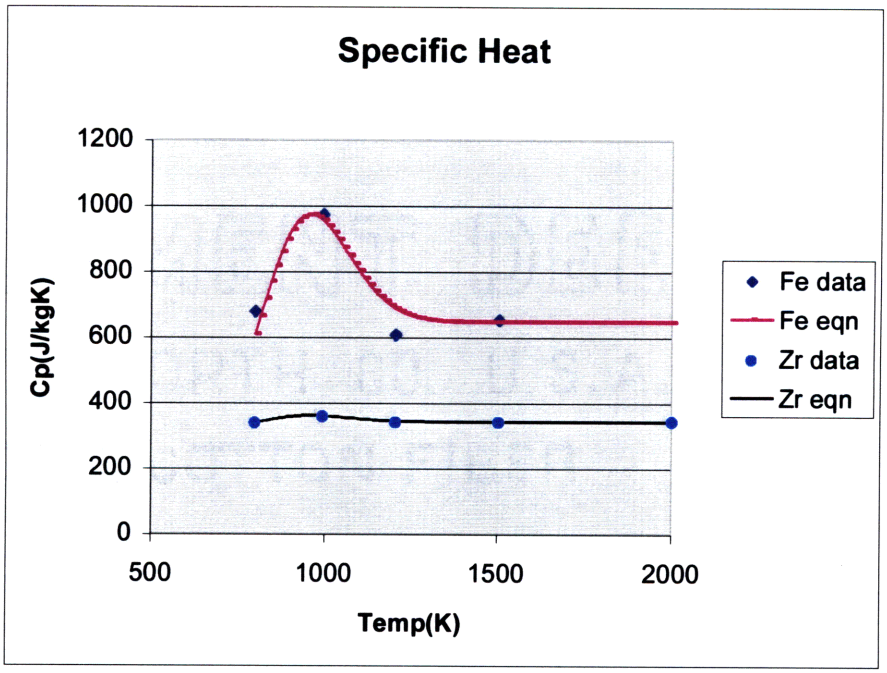

Figure C1: Metal Specific Heat Temperature Variation

Several lumped parameters for the pellets were generated by assuming that the mass percentage of the certain metal (40.5% Zr, 25% Fe, 24.5% Mn, and 10% Al) also contributed the same percentage of input into the particular characteristic. This was used for both the specific heat and the thermal conductivity to give respective values of 561 J/kgK (at 1200 K) and 38 W/mK.

Ideal Loading

Ideal theoretical loading of the pellets of 13.5 mol O_2 was obtained by assuming that all of the available zirconium, manganese, and iron oxidized. The aluminum was assumed not to oxidize and behave simply as a binder because of its low melting point of 660°C. The St-909 pellets have an initial mass of 0.6 g and are composed of 40.5% Zr, 25 % Fe, and 24.5% Mn by mass. Using their molar masses given in Table C2, the amount of moles per metal per pellet is even at 2.675E-3 mol/pellet. If each mole of Zr, Fe, and Mn fully oxidizes with one mole of oxygen, there are 8.025E-3 mol O_2 reacting, and ideal loading of 13.5 mol O_2/kg St-909 is achieved.

Appendix D: Stainless Steel Emissivity versus Temperature

The emissivity of stainless steel varies greatly with both temperature and surface conditions. For example, polished stainless steel at 600K has an emissivity of 0.19, and highly oxidized stainless steel at 1200K has an emissivity of 0.76. Table D1 below gives tabulated values for selected temperatures and surface finishes as given in Incropera (1990).

Table D1: Stainless Steel Emissivity Temperature Variation

Description	600K	800K	1000K	1200K
Polished	0.19	0.23	0.3	
Cleaned	0.24	0.28	0.35	
Lightly Oxidized		0.33	0.4	
Heavily Oxidized		0.67	0.7	0.76

While at lower temperatures emissivity variations can be considered linear, at the desired operating temperatures (900-1100K) the variation is more closely approximated as exponential. Throughout the experiment, the surface condition of the container changed. Near the beginning of the experiment it was clean, and it is assumed that the container oxidized linearly for the duration of the main part of the experiment to a state resting in between light and heavy oxidation. Figure D1 shows the emissivity for clean and heavily oxidized surface conditions. The equation for medium oxidation lies between the two extremes.

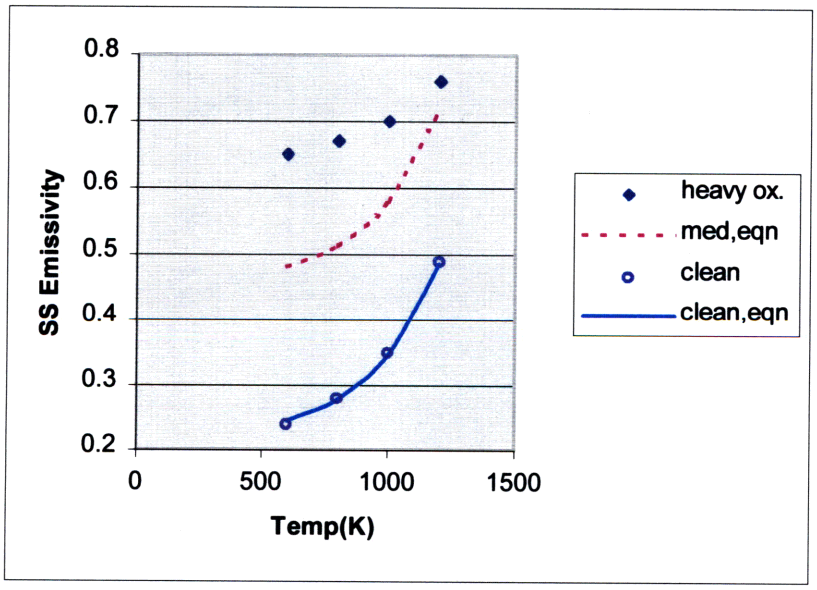

Figure D1: Stainless Steel Temperature and Surface Condition Emissivity Variation

The graph above is described by Equation D1:

$$\varepsilon = offset + 0.00696 \exp\left(\frac{T - 200}{273.07}\right) \qquad \text{(D1)}$$

where the standard deviation from the clean data and the predicted equation is 4.2×10^{-3} (~1%). The *offset* varies with the surface condition according to D2:

$$offset = \begin{cases} 0.215 & \textbf{Clean} \\ 0.269 & \textit{Light Oxidation} \\ 0.450 & \textit{Medium Oxidation} \\ 0.600 & \textit{Heavy Oxidation} \end{cases} \tag{D2}$$

Therefore, by using Equation D1 and considering the increasing emissivity effect of increased oxidation, the emissivity can be modeled as a function of time and temperature.

Appendix E: Axisymmetric Model C code

The following C code was used to solve the axisymmetric model of the St-909 getter bed. There were 200 sections within the bed comprised of 50 down the length of the bed and four radial sections with equal cross-sectional areas (a, b, c, and d). Each section had a fluid temperature node and a solid temperature node. There were also 50 wall temperature nodes. In the program, the integer i (or n) was looped through all of the axial positions (0-49), or it looped through the slices. The integer nn took on the values of 0 for radial section a, 50 for radial section b, 100 for radial section c, and 150 for radial section d. The solid temperatures were all 200 above the fluid temperatures. Table E1 summarizes the node temperatures and masses of the oxygen within the pellets.

Table E1: Axisymmetric Node Temperatures and Masses

Radial	Section	Fluid Temp #s	Solid Temp #s	Mass,O_2 #s
a	0--49	0--49	200--249	0--49
b	50--99	50--99	250--299	50--99
c	100--149	100--149	300--349	100--149
d	150--199	150--199	350--399	150--199

Code:

```
#include <stdio.h>
#include <math.h>
#define dl 0.00362204
#define Ra 0.01767
#define Rb 0.02479
#define Rc 0.030283
#define Rd 0.034925
#define Tinf 948
#define Toutlet 923.0
#define max .6
                                              /*Prototypes*/
void initialize(float *T,float *Tw,float *Tl,float *R,float *eb,
                  float *Ac);
void mass(float *M,float *prev_M,float R,float t,float *T,float *deltat,
          int nn,int i,int slice,float *time,int *newslice);
float radius(float M);
float totalMass(float *M);
void LinerTemp(float *Tl,float Tw,float T,float c11,float c12,int i);
void TubeTemp(float *Tb,float *T,int i);
void WallTemp(float *Tw,float T,float c9,float c11,float cap,int i);
void Tfluid(float c1,float c2,float c3,float c4,float c11,
            float Tinlet,float *T,float Tl,int i,int nn);
void Tsolid(float c2,float c5,float c6,float c7,float c8,float *T,
            float *Tb,float *M,int i,int nn);
float Voleff(float M);
float Volact(float M);
void constant1(float *c1,float *T,int i,int nn,float eb,float Ac);
void constant2(float *c2,float *T,float *M,float *prev_M,int i,
               int nn,float eb,float Ac);
float Cpfluid(float T);
void constant3(float *c3,float *T,float *M,float *prev_M,int i,int nn);
```

```
void constant4(float *c4,float *T,float *M,float *prev_M,int i,int nn);
void constant5(float *c5,float *T,float *M,int nn,int i);
void constant6(float *c6,float *T,float *M,float *prev_M,int i,int nn);
float tildaC(float T);
void constant7(float *c7,float *T,float *M,int i,int nn,float bed,float
Ac);
void constant9(float *c9,float Tw);
float constant10(float *T,float *M,int i,int nn,float r0,float r1,float
r2);
void constant11(float *c11,float *T,int i,float Dliner);
void constant12(float *c12,float Tl,float Tw,float Dliner);

void main()         /*Valerie Hovland, 2D Fin.Diff.Model of Packed Bed*/
{
  static float R[200],M[200]={0},T[400],Tw[50],Tb[50],Tl[50],total_M=0;
  static float
c1,c2,c3,c4,c5,c6,c7,c8,c9,c11,c12,prev_M[200]={0},brkthru=0;
  static float totalt,dt,t=0,mdotin=7.138E-5,time[200],deltat[200];
  static float eb[50],Ac[50],Acinit=2.7428E-3,Tinlet,Tfrit=933;
  static float Veff,Vact,Vtot,Vinit=9.9347E-6,Vmax=13.76E-6,Dliner;
  int print_interval,i,ii,slice=0,n=0,nn,newslice=0;
  FILE *fpo;

  totalt=10000;         /*total time in seconds*/

  dt=1;/*time steps*/
  print_interval=60;    /*print to file every 'x' seconds*/

  initialize(T,Tw,Tl,R,eb,Ac);      /*initial bed temperatures*/
  Vtot=Vinit;

  fpo=fopen("bed2d.out", "w");      /*open output file*/
  fprintf(fpo, "Packed Bed Temperatures\t\t\t");
  fprintf(fpo, "\nTime(s)\tM,O2(kg)\tBreakthru(kg)\t");
  for(i=200;i<=399;i++)             /*headers for the file*/
    fprintf(fpo,"T[%d](C)\t", i);
  fprintf(fpo,"\t");
  for(i=0;i<=49;i++)
    fprintf(fpo,"Tw[%d](C)\t",i);

  ii=print_interval;
  while(t<=totalt) {
    if(ii==print_interval){         /*print to file at intervals*/
      fprintf(fpo,"\n%f\t%2.6e\t%.5e",t,total_M,brkthru);
      for(i=200;i<=399;i++)
        fprintf(fpo,"\t%f",T[i]-273);   /*print temperatures*/
      fprintf(fpo,"\t");
      for(i=0;i<=49;i++)
        fprintf(fpo,"\t%f",Tw[i]-273);  /*print wall temp*/
      fprintf(fpo,"\t");
      ii=0;
    }

    n=-1;
    while(n<=48)                    /*loop through slices*/
      {                 /*loop until all input mass is gettered*/
      total_M=totalMass(M);
```

```
  brkthru=mdotin*t-total_M;     /*total mass breakthrough in kg*/
  if(brkthru>=0)
    n++;   /*end up starting at n=0 and going until n=49*/
  else break;
  for(nn=0;nn<=150;nn+=50)
    {                            /*loop over radials a,b,c,d*/
      prev_M[nn+n]=M[nn+n];      /*keep track of previous mass*/
      slice=n;
      mass(M,prev_M,R[nn+n],t,T,deltat,nn,n,slice,time,&newslice);
                          /*gives mass in kg of a single 909 pellet*/
      R[nn+n]=radius(M[nn+n]);  /*gives radius of single pellet (m)*/
    }
  }

for(i=49;i>=0;i--)
  TubeTemp(Tb,T,i);             /*find inlet tube temperatures*/
  Tfrit=705+180*(t/3600-.3)*exp(-2*pow(t/3600-.3,2))+273;
  Tinlet=.4194*(Tb[0]-Tfrit)+Tfrit;
        /*inlet temperature of bed is end of bulk tube flow,
  increased*/
         /*due to flowing through frit*/

for(i=0;i<=49;i++){             /*loop over all axial slices i*/
  Veff=Voleff(M[i]);            /*effective volume of pellets*/
  if(Veff<Vinit)                /*calculate swelling*/
    Ac[i]=Acinit;
  else {
    Vtot=Veff;
    Ac[i]=Vtot/dl;
  }
  Vact=Volact(M[i]);
  eb[i]=(Vtot-Vact)/Vtot;
  Dliner=pow(1.27324*Ac[i],.5);  /*diameter of liner*/

  if(Veff<Vmax){/*when swelling has not pushed liner to ID of primary*/
    constant9(&c9,Tw[i]);
    constant11(&c11,T,i,Dliner);
    constant12(&c12,Tl[i],Tw[i],Dliner);
    LinerTemp(Tl,Tw[i],T[150+i],c11,c12,i); /*find liner temperature*/
    WallTemp(Tw,Tl[i],c9,c12,13.44,i);      /*find wall temperatures*/
  }
  else {
    constant9(&c9,Tw[i]);
    constant11(&c11,T,i,Dliner);
    WallTemp(Tw,T[150+i],c9,c11,16.74,i);   /*find wall temperature*/
    Tl[i]=Tw[i];/*when swelling pushes liner to wall, temps are same*/
  }

  for(nn=0;nn<=150;nn+=50) {          /*loop over radial sections*/
    constant1(&c1,T,i,nn,eb[i],Ac[i]);/*find temp-varying constants*/
    constant2(&c2,T,M,prev_M,i,nn,eb[i],Ac[i]);
    constant3(&c3,T,M,prev_M,i,nn);
    constant4(&c4,T,M,prev_M,i,nn);
    constant5(&c5,T,M,nn,i);
    constant6(&c6,T,M,prev_M,i,nn);
    constant7(&c7,T,M,i,nn,eb[i],Ac[i]);
    c8=c7;
```

```
        Tsolid(c2,c5,c6,c7,c8,T,Tb,M,i,nn+200); /*find solid temperature*/
        Tfluid(c1,c2,c3,c4,c11,Tinlet,T,Tl[i],i,nn);/*find fluid temp*/
      }
    }
    t=t+dt;                          /*increment time*/
    ii=ii+dt;                        /*increment print interval counter*/
    total_M=totalMass(M);
  }
  fclose(fpo);

  return;
}



void initialize(float *T,float *Tw,float *Tl,float *R,float *eb,float *Ac)
{
  float temp;
  int i,nn;
  FILE *fpi;

  fpi=fopen("initial2d.txt", "r");        /*open temperature file*/
  for(i=0;i<=199;i++){                    /*loop over slices*/
    fscanf(fpi,"%f",&temp);               /*initial temperatures in
Kelvin*/
    T[i]=temp+273;
    T[200+i]=temp+273;                /*initial solid=initial fluid temps*/
  }
  for(i=0;i<=49;i++){
    fscanf(fpi,"%f",&temp);
    Tw[i]=temp+273;
    Tl[i]=Tw[i];
  }
  fclose(fpi);
  for(i=0;i<=199;i++)
    R[i]=0.003;               /*initial radius of a pellet is 3mm*/
  for(i=0;i<=49;i++)
    {
      eb[i]=.476;              /*initial void fraction*/
      Ac[i]=.0027428;         /*initial cross sectional area*/
    }
  return;
}

void mass(float *M,float *prev_M,float R,float t,float *T,float *deltat,
          int nn,int n,int slice,float *time,int *newslice)
{                                   /*mass in a single pellet*/
  float tmp=0.0,D,avgdens,Mtot,tstar=0,x;
  float C1,C2,Mgettered=0,M2getter,ratio;
  int i,k;

  D=4.744E-9*exp(-1670.54/T[nn+n+200]);   /*diffusion coeff, temp
variance*/
  if(*newslice<slice){        /*keep track of start times for each slice*/
    for(i=0;i<=150;i+=50)     /*start times same for a,b,c,d of slice n*/
      time[slice+i]=t;
```

```
    *newslice=slice;
  }

  Mtot=2.592E-4;
  Mgettered=totalMass(prev_M);  /*previous mass gettered by entire bed*/
  for(i=0;i<=(n-1);i++) {          /*sum NEW mass over previous slices*/
    for(k=0;k<=150;k+=50)          /*for each slice, sum over a,b,c,d*/
      Mgettered+=11.5*(M[k+i]-prev_M[k+i]);
  }
  M2getter=7.138E-5*t-Mgettered;          /*mass into getter slice*/
  ratio=M2getter/7.138E-5;          /*7.138E-5 kg into bed per dt=1sec*/
  if(ratio>0 && ratio<=1)
    Mtot=ratio*Mtot;   /*total mass related to input slice concentration*/
  if(ratio>1)
    Mtot=1*Mtot;        /*max the mtot can reach is max loading Mtot*/

  C1=.997932;
  C2=2.467401/(R*R);

  if(Mtot>0)
    x=1/C1*(1-M[nn+n]/Mtot);        /*adjust for discontinuities in mass*/
  else                             /*when the diff coeff changes with temp*/
    x=1/C1;
  tstar=time[nn+n]-1/(C2*D)*log(x);       /*log=ln*/
  deltat[nn+n]=t-tstar;       /*deltat is the time difference at given*/
                              /*masses for different temperatures*/

  tmp=C1*exp(-2.467401*D/(R*R)*(t-time[nn+n]-deltat[nn+n]+1));
  M[nn+n]=Mtot*(1-tmp);       /*mass of a single pellet for section nn+n*/
  return;                     /*nn=0(a),50(b),100(c),150(d) and slice n*/
}

float radius(float M)
{
  float SA;

  SA=.0001319;                /*initial surface area,m^3*/
  return sqrt(SA/14.66*(1+4153.33*M));    /*returns raduis*/
}

float totalMass(float *M)
{
  float sum=0;
  int i;

  for(i=0;i<=199;i++)
    sum+=11.5*M[i];           /*11.5 pellets per 200 sections*/
  return sum;
}

void TubeTemp(float *Tb,float *T,int i)
{
  if(i==49)              /*the first section for the inlet tube*/
    Tb[i]=.985*(273+400-T[200+i])+T[200+i];
  else                   /*transfers heat from the solid temperature*/
    Tb[i]=.985*(Tb[i+1]-T[200+i])+T[200+i];
  return;
```

```
}

void LinerTemp(float *Tl,float Tw,float T,float c11,float c12,int i)
{
  float K[2],dt=1,cap=3.3;    /*cap is the heat capacity of the liner*/

  K[0]=c11+c12;
  K[1]=c11*T+c12*Tw;

  Tl[i]=(K[1]+(K[0]*Tl[i]-K[1])*exp(-1*K[0]*dt/cap))/(K[0]);
  return;
}

void WallTemp(float *Tw,float T,float c9,float c11,float cap,int i)
{
  float K[2],dt=1;

  K[0]=c9+c11;
  K[1]=c9*Tinf+c11*T;

  Tw[i]=(K[1]+(K[0]*Tw[i]-K[1])*exp(-1*K[0]*dt/cap))/(K[0]);
  return;
}

void Tfluid(float c1,float c2,float c3,float c4,float c11,
            float Tinlet,float *T,float Tl,int i,int nn)
{
  float K[2],dt=1;

  if(nn!=150)
    c11=0;              /*wall heat transfer only for d sections*/
  if(i!=0 && i!=49){
    K[0]=c2+c3+c4+c11;
    K[1]=c2*T[nn+i+200]+c3*T[nn+i-1]+c4*T[nn+i+1]+c11*Tl;
  }
  if(i==0) {                  /*first slice*/
    K[0]=c2+c3+c4+c11;
    K[1]=c2*T[nn+i+200]+c3*Tinlet+c4*T[nn+i+1]+c11*Tl;
  }
  if(i==49) {                   /*last slice*/
    T[nn+i]=Toutlet;
    return;
  }
  T[nn+i]=(-1*K[1]+(-1*K[0]*T[nn+i]+K[1])*exp(-1*K[0]*dt/c1))/(-1*K[0]);
  return;
}

void Tsolid(float c2,float c5,float c6,float c7,float c8,float *T,
            float *Tb,float *M,int i,int nn)
{
  float K[2],dt=1,condin,condout,conv;

  if(nn==200) {               /* a slices*/
    conv=0.00497;/*no in radial conduction for a slices--tube convec*/
    condout=constant10(T,M,i,nn,0,Ra-.00635,Rb);
  }
  if(nn==250) {
```

```
    condin=constant10(T,M,i,nn,0,Ra,Rb);
    condout=constant10(T,M,i,nn,Ra,Rb,Rc);
  }
  if(nn==300) {
    condin=constant10(T,M,i,nn,Ra,Rb,Rc);
    condout=constant10(T,M,i,nn,Rb,Rc,Rd);
  }
  if(nn==350) {
    condin=constant10(T,M,i,nn,Rb,Rc,Rd);
    condout=0;                    /*no out radial cond for d slices*/
  }


  if(i!=0 && i!=49) {          /*expect 0<i<49*/
    if(nn!=200 && nn!=350){
      K[0]=c2+c7+c8+condin+condout;
      K[1]=c6+c2*T[nn+i-200]+c7*T[nn+i-1]+c8*T[nn+i+1]+condin*T[nn+i-50]+
        condout*T[nn+i+50];
    }
    if(nn==200){         /*a slices*/
      K[0]=c2+c7+c8+condout+conv;
      K[1]=c6+c2*T[nn+i-200]+c7*T[nn+i-1]+c8*T[nn+i+1]+condout*T[nn+i+50]
      +conv*Tb[i];
    }
    if(nn==350){         /*d slices*/
      K[0]=c2+c7+c8+condin;
      K[1]=c6+c2*T[nn+i-200]+c7*T[nn+i-1]+c8*T[nn+i+1]+condin*T[nn+i-50];
    }
  }
  if(i==0){        /*first slice: no in axial conduction*/
    if(nn!=200 && nn!=350){
      K[0]=c2+c8+condin+condout;
      K[1]=c6+c2*T[nn+i-200]+c8*T[nn+i+1]+condin*T[nn+i-
50]+condout*T[nn+i+50];
    }
    if(nn==200){  /*no in radial conduction for a section*/
      K[0]=c2+c8+condout+conv;
      K[1]=c6+c2*T[nn+i-200]+c8*T[nn+i+1]+condout*T[nn+i+50]+conv*Tb[i];
    }
    if(nn==350){  /*no out radial conduction for d section*/
      K[0]=c2+c8+condin;
      K[1]=c6+c2*T[nn+i-200]+c8*T[nn+i+1]+condin*T[nn+i-50];
    }
  }
  if(i==49){       /*last slice: no out axial conduction*/
    if(nn!=200&&nn!=350){
      K[0]=c2+c7+condin+condout;
      K[1]=c6+c2*T[nn+i-200]+c7*T[nn+i-1]+condin*T[nn+i-50]
            +condout*T[nn+i+50];
    }
    if(nn==200){  /*no in radial conduction for a section*/
      K[0]=c2+c7+condout+conv;
      K[1]=c6+c2*T[nn+i-200]+c7*T[nn+i-1]+condout*T[nn+i+50]+conv*Tb[i];
    }
    if(nn==350){  /*no out radial conduction for d section*/
      K[0]=c2+c7+condin;
      K[1]=c6+c2*T[nn+i-200]+c7*T[nn+i-1]+condin*T[nn+i-50];
```

```
    }
  }
  T[nn+i]=(-1*K[1]+(-1*K[0]*T[nn+i]+K[1])*exp(-1*K[0]*dt/c5))/(-1*K[0]);
  return;
}

float Voleff(float M)
{                          /*returns effective pellet volume*/
  float Vinit=5.20247E-6;  /*initial volume of 46 pellets*/

  return Vinit*(1+2*(1-exp(-4468.75*M)));
}

float Volact(float M)
{                          /*returns actual pellet volume*/
  float Vinit=5.20247E-6;

  return Vinit*(1+1.8*(1-exp(-2062.5*M)));
}

void constant1(float *c1,float *T,int i,int nn,float eb,float Ac)
{                              /*heat capacity term for fluid*/
  float rho;

  rho=.142178+1.103286*exp(-.00165*T[nn+i]);/*calculate density*/
  *c1=dl*eb*Ac/4*rho*Cpfluid(T[nn+i]);/*fluid transient term*/
  return;                      /*area goes to Ac/4*/
}

void constant2(float *c2,float *T,float *M,float *prev_M,int i,
               int nn,float eb,float Ac)
{                              /*convection term*/
  int n,k;
  float Mflow=0,Temp,Re,mu,dt=1,kair,Perim,Dh,L;
  float Mdotin=3.22669E-4,hp;

  Temp=(T[nn+i]+T[nn+i+200])/2; /*evaluate mu,k at average pellet/fluid
temp*/
  Ac=Ac/4;        /*cross section area divided by four for a,b,c,d*/

  for(n=0;n<=(i-1);n++)
    for(k=0;k<=150;k+=50)
      Mflow+=11.5*(M[k+n]-prev_M[k+n])/dt;/*oxygen gettered by prev slices*/
  Perim=1166.66*(1-eb)*Ac;        /*transfer perimeter*/
  Dh=eb/(1166.66*(1-eb));         /*hydraulic diameter*/
  L=6*Dh;          /*characteristic length of packed bed systems*/
  mu=(16+.02528333*Temp)*1E-6;    /*viscosity temp variance*/

  Re=L/eb/Ac*(Mdotin-Mflow)/4/mu;    /*Reynolds number,below valid
20<Re<7600*/
  if(Re<20)
      Re=20;          /*correcting for non linear log behavior*/
  kair=.015+5.1666E-5*Temp;    /*thermal conductivity of air*/
  hp=kair/L*pow(.7,.3333)*(.5*pow(Re,.5)+.2*pow(Re,.6666));

  *c2=hp*Perim*dl;/* c2=hp*P*dl */
  return;
```

```
}

float Cpfluid(float T)
{               /*calculates heat capacity of fluid at various
temperatures*/
  return 891.3907+495.6262*(1-exp(-.00636*T));/*J/kg K*/
}

void constant3(float *c3,float *T,float *M,float *prev_M,int i,int nn)
{                                       /*mdotCp term for air, left*/
  float Temp=0,Mflow=0,dt=1,mflowtot=3.22669E-4;
  int n,k;

  Temp=(T[nn+i]+T[nn+i+200])/2;/*evaluate cp at avg pellet/fluid temp*/

  for(n=0;n<=(i-1);n++)
    for(k=0;k<=150;k+=50)
      Mflow+=11.5*(M[k+n]-prev_M[k+n])/dt;/*oxygen gettered by prev slices*/
  *c3=(mflowtot-Mflow)/4*Cpfluid(Temp);  /* c3=(mdot*cp)left*/
  return;
}

void constant4(float *c4,float *T,float *M,float *prev_M,int i,int nn)
{                                       /*mdotCp term for air,right*/
  float Temp=0,Mflow=0,dt=1,mflowtot=3.22669E-4;/*tot in:3.22669E-4 kg/s*/
  int n,k;

  Temp=(T[nn+i]+T[nn+i+200])/2;
            /*evaluate heat capacity at average pellet/fluid temp*/
  for(n=0;n<=i;n++)
    for(k=0;k<=150;k+=50)
      Mflow+=11.5*(M[k+n]-prev_M[k+n])/dt;/*oxygen gettered by prev slices*/
  *c4=(mflowtot-Mflow)/4*Cpfluid(Temp);  /* c4=(mdot*cp)right*/

  return;
}

void constant5(float *c5,float *T,float *M,int nn,int i)
                        /*heat capacity term for pellets*/
{
  float cpZr,cpFe,cpAl,Temp,Mass;

  Temp=T[nn+i+200];      /*temperature of solid section*/
  Mass=0.6E-3+M[nn+i];   /*mass of a single pellet within
section=.6g+MO2*/

  cpZr=.2045*(Temp-810)*exp(-1*pow((Temp-810),2)/44000)+344;
  cpFe=3.636*(Temp-810)*exp(-1*pow((Temp-810),2)/44000)+647.7;
  cpAl=1200;         /*specific heats in J/kgK*/

  *c5=11.5*Mass*(.405*cpZr+.495*cpFe+.1*cpAl);
  if(nn==200)     /*for inner a sections, have added capacity*/
    *c5+=0.3;     /*for inner tube*/
  *c5+=1.5;
  return;         /*11.5 pellets per section*/
}
```

```
void constant6(float *c6,float *T,float *M,float *prev_M,int i,int nn)
{
  int n=11.5;     /* n=#pellets per section*/

  *c6=n*tildaC(T[nn+i+200])*(M[nn+i]-prev_M[nn+i]);
                        /*heat generated per slice*/
  return;
}

float tildaC(float T)
{
  float Zr,Mn,Fe;       /*energy released per kg oxidized*/
                  /*dG=A+BT+CTlogT, enthalpy: dH=A-CT/ln(10)*/
  Zr=-(-1100032+7.56*T/log(10));
  Mn=-(-383209-2.15*T/log(10));
  Fe=-(-270590+1.26*T/log(10));

  return 10.3*(Zr+Mn+Fe);
}

void constant7(float *c7,float *T,float *M,int i,int nn,float eb,float Ac)
{                              /*axial conductivity term*/
  float n,ks=31.5,kf,keff;    /*ks=thermal conductivity of pellet*/
  float mu,rho,Re,tmp;

  kf=.015+5.1666E-5*T[nn+i+200];    /*thermal conductivity of air*/
  n=.28-.757*log10(eb)-.057*log10(ks/kf);/*exponent for effective
conductivity*/
  keff=kf*pow((ks/kf),n);           /*effective radial thermal cond*/

  mu=(16+.02528333*T[nn+i])*1E-6;         /*viscosity temp variance*/
  rho=.142178+1.103286*exp(-.00165*T[nn+i]);    /*density temp variance*/
  Re=3.9144E-4*rho/mu;                    /*Reynold's number*/

  keff=kf*(keff/kf+.5*Re*0.7);            /*effective axial cond*/

  *c7=mult7*Ac/4*keff/dl;
  return;
}

void constant9(float *c9,float Tw)
{                                  /*radiation to heater term*/
  float Tm; /*radiate to heater 675=948K*/
  float offset=max,e;
  float Aouter=.04864,sigma=5.67E-8;

  e=offset+.00696*exp((Tw-200)/273.07);   /*emissivity temp variance*/
  e=1/(1/e+1.058);/*e12=1/(1/e1+A1/A2*(1/e2-1))*/

  Tm=(Tw+Tinf)/2;             /*mean temperature between wall and coil*/

  *c9=1.5*4*e*sigma*Aouter/50*pow(Tm,3);
  return;
}

float constant10(float *T,float *M,int i,int nn,float r0,float r1,float
r2)
```

```
{                                       /*radial pellet conductivity term*/
  float n,ks=31.5,kf,keff,c10;          /*ks=thermal conductivity of pellet*/
  float ro,ri;

  kf=.015+5.1666E-5*T[nn+i+200];        /*thermal conductivity of air*/
  n=.28-.757*log10(.4)-.057*log10(ks/kf);/*exponent for eff conductivity*/
  keff=kf*pow((ks/kf),n);                   /*effective thermal cond*/

  ri=(r0+r1)/2;          /*taking resistance at middle of sections*/
  ro=(r1+r2)/2;

  c10=35*6.28318*dl*keff/log(ro/ri);
  return c10;
}

void constant11(float *c11,float *T,int i,float Dliner)
{                                  /*wall heat tranfer term*/
  float hw,Re,A;
  float n,ks=31.5,kf,mu,rho;

  A=3.14159*Dliner*dl;          /*outer area =pi*D*dl*/

  kf=.015+5.1666E-5*T[150+i]; /*thermal conductivity of air*/

  mu=(16+.02528333*T[150+i])*1E-6;    /*viscosity temp variance*/
  rho=.142178+1.103286*exp(-.00165*T[150+i]);/*density temp variance*/
  Re=3.9144E-4*rho/mu;                /*Reynolds number*/

  if(Re<20)
      Re=20;             /*correct for limiting Nu behavior*/
  hw=kf/.006*0.16*pow(Re,.93);/*wall heat transfer coefficient*/

  *c11=10*hw*A;
  return;
}

void constant12(float *c12,float Tl,float Tw,float Dliner)
{                         /* Radiation from liner to wall*/
  float Tm;
  float offset=.6,el,ew,e;
  float Aouter,sigma=5.67E-8;

  Aouter=3.14159*Dliner*dl;                 /*outer area of liner*/
  el=offset+.00696*exp((Tl-200)/273.07);  /*emissivity temp var of liner*/
  ew=offset+.00696*exp((Tw-200)/273.07);  /*emissivity temp var of wall*/
  e=1/(1/el+Dliner/.06985*(1/ew-1));      /*e12=1/(1/e1+A1/A2*(1/e2-1))*/

  Tm=(Tl+Tw)/2;          /*mean temperature between liner and wall*/

  *c12=1.5*4*e*sigma*Aouter*pow(Tm,3);
  return;
}
```